Atmospheric
Chemistry
and Physics

Open Access

Multi-model simulation of CO and HCHO in the Southern Hemisphere: comparison with observations and impact of biogenic emissions

G. Zeng[1], **J. E. Williams**[2], **J. A. Fisher**[3], **L. K. Emmons**[4], **N. B. Jones**[3], **O. Morgenstern**[1], **J. Robinson**[1], **D. Smale**[1], **C. Paton-Walsh**[3], and **D. W. T. Griffith**[3]

[1]National Institute of Water and Atmospheric Research, Lauder, New Zealand
[2]Royal Netherlands Meteorological Institute, De Bilt, the Netherlands
[3]University of Wollongong, Wollongong, New South Wales, Australia
[4]National Centre for Atmospheric Research, Boulder, Colorado, USA

Correspondence to: G. Zeng (guang.zeng@niwa.co.nz)

Abstract. We investigate the impact of biogenic emissions on carbon monoxide (CO) and formaldehyde (HCHO) in the Southern Hemisphere (SH), with simulations using two different biogenic emission inventories for isoprene and monoterpenes. Results from four atmospheric chemistry models are compared to continuous long-term ground-based CO and HCHO column measurements at the SH Network for the Detection of Atmospheric Composition Change (NDACC) sites, the satellite measurement of tropospheric CO columns from the Measurement of Pollution in the Troposphere (MOPITT), and in situ surface CO measurements from across the SH, representing a subset of the National Oceanic and Atmospheric Administration's Global Monitoring Division (NOAA GMD) network. Simulated mean model CO using the Model of Emissions of Gases and Aerosols from Nature (v2.1) computed in the frame work of the Land Community Model (CLM-MEGANv2.1) inventory is in better agreement with both column and surface observations than simulations adopting the emission inventory generated from the LPJ-GUESS dynamical vegetation model framework, which markedly underestimate measured column and surface CO at most sites. Differences in biogenic emissions cause large differences in CO in the source regions which propagate to the remote SH. Significant inter-model differences exist in modelled column and surface CO, and secondary production of CO dominates these inter-model dif-

ferences, due mainly to differences in the models' oxidation schemes for volatile organic compounds, predominantly isoprene oxidation. While biogenic emissions are a significant factor in modelling SH CO, inter-model differences pose an additional challenge to constrain these emissions. Corresponding comparisons of HCHO columns at two SH mid-latitude sites reveal that all models significantly underestimate the observed values by approximately a factor of 2. There is a much smaller impact on HCHO of the significantly different biogenic emissions in remote regions, compared to the source regions. Decreased biogenic emissions cause decreased CO export to remote regions, which leads to increased OH; this in turn results in increased HCHO production through methane oxidation. In agreement with earlier studies, we corroborate that significant HCHO sources are likely missing in the models in the remote SH.

1 Introduction

Carbon monoxide (CO) is ubiquitous throughout the troposphere and is an important ozone (O_3) precursor; it originates from both primary emission sources (fossil fuel and biomass combustion, biogenic, and oceanic processes) and in situ chemical production. The dominant chemical source term in the troposphere is the photo-oxidation of methane (CH_4)

and non-methane volatile organic compounds (NMVOCs) (e.g. Duncan et al., 2007). Its principal sink is the reaction with the hydroxyl radical (OH); hence, CO plays a key role in controlling the oxidizing capacity in the atmosphere (e.g. Levy, 1971). The oxidation of methane and NMVOCs, such as isoprene (C_5H_8), monoterpenes ($C_{10}H_{16}$), acetone (CH_3COCH_3) and higher aldehydes, leads to the formation of formaldehyde (HCHO), which, through photolysis and reaction with OH, is the major chemical source of CO (Atkinson, 2000). Once formed, CO has a relatively long lifetime of around 1–2 months, and therefore it is often used as a chemical marker for characterizing the long-range transport of air pollutants away from important source regions (e.g. Staudt et al., 2001; Heald et al., 2003; Liang et al., 2004; Fisher et al., 2010).

Due to a lack of strong regional emission sources, the Southern Hemisphere (SH) acts as a global sink for many of the polluting trace species emitted in the tropics, where polluted plumes are transported away out over the relatively clean ocean becoming subject to chemical processing. The relatively low population density, and thus low anthropogenic activity, in the SH means that direct emission sources of CO are principally limited to biomass burning (BB) and direct biogenic processes (e.g. Swinnerton et al., 1970; Watson et al., 1990; Fishman et al., 1991). Satellite and ground-based observations of CO in the SH have been used to identify the effect of BB and its footprint through long-range transport in the SH, which dominates the CO seasonal cycle there (e.g. Rinsland et al., 2005; Edwards et al., 2006; Gloudemans et al., 2006; Morgenstern et al., 2012). Global distributions of HCHO are much more inhomogeneous than CO, due to the much shorter lifetime of HCHO (on the order of a few hours), and the concentration of HCHO drops off sharply away from the source regions. Observations of HCHO are commonly used to constrain isoprene emissions in high-emission regions, because it is a high-yield product of isoprene oxidation (e.g. Palmer et al., 2003; Shim et al., 2005; Barkley et al., 2008).

Global chemical models have been extensively used to estimate the sources and sinks of CO (e.g. Holloway et al., 2000; Duncan et al., 2007). However, systematic discrepancies between modelled and observed CO still exist, with models generally underestimating CO in the more polluted Northern Hemisphere (NH) and overestimating CO in the SH (e.g. Shindell et al. , 2006; Naik et al., 2013; Stein et al., 2014). In the remote SH, however, the extremely low HCHO concentrations are expected to further complicate the comparisons of model results with observations.

In contrast to the anthropogenic emissions dominating CO sources in the more polluted NH, biogenic volatile organic compounds (VOCs) are important sources of CO and HCHO in the SH, and isoprene oxidation contributes significantly to the regional CO and HCHO abundances in this region (Pfister et al., 2008). However, large uncertainties exist in biogenic emissions inventories, in particular for surface fluxes of iso-

prene and monoterpenes (Arneth et al., 2008). Bottom-up estimates of annual isoprene emissions vary between 400 and 600 Tg C yr^{-1} (Arneth et al., 2008), and the typical range of annual total isoprene emissions implemented in global atmospheric chemistry models is $\sim$ 200–600 Tg C yr^{-1} (Stevenson et al., 2006). The effect of such uncertainties in biogenic emissions on SH composition, such as CO and HCHO, has not been adequately assessed. Moreover, the sparsity of the ground-based CO and HCHO measurements in the SH also limits our ability to constrain these biogenic emissions.

In this study, we perform a number of simulations using an ensemble of chemical transport models (CTMs) and chemistry–climate models (CCMs) as part of the Southern Hemisphere Model Intercomparison Project (SHMIP), to compare modelled CO and HCHO to observations and to investigate the factors that influence the distributions of CO and HCHO in the SH. Given the relatively low anthropogenic emissions in the SH and the dominance of biogenic emissions of VOCs (mainly isoprene), we determine the influence that different emission inventories of isoprene and monoterpenes have regarding their effects on modelled CO and HCHO columns in the SH. Satellite observations of SH CO usually are in good agreement with ground-based observations; however, the data quality of the satellite data deteriorates towards the poles (Morgenstern et al., 2012). Morgenstern et al. (2012) found that CO columns exhibit a large-scale mode of variability in the remote SH that does not exist in the NH. For our purposes, we make use of high-precision ground-based Fourier transform infrared spectroscopy (FTIR) measurements of CO columns from four SH sites that have not previously been fully exploited for model evaluations, namely Darwin (12.43° S, 130.89° E) and Wollongong (34.41° S, 150.88° E) in Australia, Lauder (45.04° S, 169.69° E) in New Zealand, and Arrival Heights (77.82° S, 166.65° E) in Antarctica. We also compare the modelled HCHO columns to those observed by the FTIR instruments at Wollongong and Lauder. In a companion paper, Fisher et al. (2015) have evaluated the vertical gradients of CO from the SHMIP models in the vicinity of Cape Grim, Australia, which is representative of SH mid-latitude background air, using multi-year aircraft measurements available from the Cape Grim Overflight Programme (Langenfelds et al., 1996). The influence of both chemistry and transport on the modelled vertical gradients of CO are addressed. Although there are biases of various magnitudes across the different models, the seasonal variability and extent of the gradients in tropospheric CO are shown to be captured reasonably well, especially during the tropical BB season.

In this paper we address the sensitivity of CO and HCHO distributions in the SH to biogenic emissions of isoprene and monoterpenes as provided by the LPJ_GUESS emission inventory (Arneth et al., 2007a, b; Schurgers et al., 2009) and the MEGANv2.1 model (Guenther et al., 2012) across the models included in SHMIP. In Sect. 2 we provide model descriptions, the common emission inventories used to drive

the models, and the observations used in the study. In Sect. 3 we compare results for the period 2004–2008 and show comparisons between modelled CO and HCHO columns and the FTIR measurements at the four SH sites mentioned above, modelled and MOPITT CO columns, as well as comparisons between modelled and observed surface CO. In Sect. 4 we analyse differences in the models' abilities to reproduce SH CO and HCHO columns, and the underlying differences in the models' chemistry and transport. In Sect. 5 we further analyse the chemical production and loss terms to address differences in models' NMVOC oxidation mechanisms. In Sect. 6 we assess the sensitivity of modelled CO and HCHO to changes in biogenic emissions and the effect of such changes on the oxidizing capacity in the clean SH. Finally, in Sect. 7 we present our conclusions.

2 Model simulations and observations

The SHMIP intercomparison uses four global models, including two CTMs (Tracer Model 5 (TM5), GEOS-Chem) and two CCMs (the Community Atmosphere Model with chemistry (CAM-chem), NIWA-UKCA – the National Institute of Water and Atmospheric Research – UK Chemistry and Aerosols Model). In this section we provide the description of the simulations performed, the common emission inventories employed, a brief description of each model, the meteorological drivers, and the observations used for evaluating the performance of the models.

2.1 Simulations

We perform simulations covering the period of 2004 to 2008 using a 1-year spin-up for 2003. The two CTMs are driven by the meteorological analysis for the same period from their respective sources, whereas NIWA-UKCA uses observed sea surface temperature and sea ice data sets. CAM-chem runs in the specified-dynamics mode, using meteorological fields from the reanalysis data. Two simulations are performed in all models with identical emission inventories for the anthropogenic and BB components, but different inventories are adopted for biogenic isoprene and monoterpene emissions. We also include passive CO tracers in the simulation defined as having the same global primary, surface emission sources as CO, but with one having a fixed lifetime of 25 days and a second having the lifetime determined by OH distribution in each respective model. These tracers allow for the differentiation of the inter-model variability with respect to transport of CO to the SH from the main source regions.

Although we have been careful to harmonize the emissions used across models, differences in the chemical mechanisms which are employed result in the aggregated emissions of the NMVOCs being somewhat different across the models. For anthropogenic emissions, we adopt the yearly specific Monitoring Atmospheric Composition and Climate

(MACC)/CITYZEN (MACCity) global emission estimates (Lamarque et al., 2010; Granier et al., 2011) nested with the Regional Emission Inventory in Asia (REASv2.1) for the East Asian region (Kurokawa et al., 2013). Interannually varying monthly mean BB emissions are taken from the Global Fire Emissions Database version 3 (GFEDv3) (van der Werf et al., 2010). For lightning-NO_x emissions, each model adopts individual parameterizations, which interact with the models' convection schemes. Natural emissions of soil NO_x and CO from the ocean are taken from the Precursors of Ozone and their Effects in the Troposphere (POET) database (http://eccad.sedoo.fr). The annual total emission fluxes for key species are listed in Table 1 for the simulation period of 2004–2008.

Biogenic emissions for isoprene, monoterpenes, CO, methanol, and acetone are based on MEGANv2.1 (Guenther et al., 2012) and are calculated offline using the Community Land Model (CLM4.0; Lawrence et al., 2011), driven by Climate Research Unit-National Centers for Environmental Prediction (CRUNCEP) reanalyses (http://dods.extra.cea.fr/data/p529viov/cruncep/readme.html) for each year. We refer to this data set as Model of Emissions of Gases and Aerosols from Nature (v2.1) computed in the frame work of the Land Community Model (CLM-MEGANv2.1) hereafter. We then replace the MEGANv2.1 emissions for isoprene and monoterpenes with the "GUESS-ES" emissions that were calculated by the LPJ-GUESS model (http://eccad.sedoo.fr) in our second set of simulations for comparison (hereafter referred to as LPJ-GUESS simulations); this emission data set is generated using the dynamical vegetation model LPJ-GUESS driven with Climate Research Unit Timeseries (CRU TS) 3.1 climate data (Arneth et al., 2007a; Schurgers et al., 2009). None of the models currently include any higher terpenes. The yearly varying annual global total emissions of isoprene from CLM-MEGANv2.1 (462–508 Tg yr^{-1}) are markedly larger than the LPJ-GUESS emissions (431–450 Tg yr^{-1}), i.e. ~ 5–10 % relative to CLM-MEGANv2.1 (Table 1). The corresponding differences are much larger for the SH between these two inventories, i.e. ~ 10–20 % relative to CLM-MEGANv2.1, over the same period. For monoterpenes, the annual total CLM-MEGANv2.1 emissions are substantially larger than the LPJ-GUESS emissions, i.e. a factor of 4 and 6 larger globally and in the SH, respectively. The two data sets have been generated from the respective land surface models driven by similar meteorological fields, as specified in the above references. Here, we do not harmonize the model meteorology to those used in generating the biogenic emissions. Instead, we prescribe the monthly mean biogenic emissions in the models to ensure the consistency. Figure 1 shows the SH and regional monthly total isoprene emission fluxes from LPJ-GUESS and CLM-MEGANv2.1 for Australia and part of Indonesia (0–44° S, 94–156° E), southern Africa (0–37° S, 9–44° E), and South America (0–57° S, 34–84° W), the regions with high isoprene emissions. The largest monthly emissions oc-

Table 1. Global annual total emissions (Tg yr^{-1}). Values in brackets are sums of SH emissions.

	2004	2005	2006	2007	2008
Total surface NO	96	98	99	101	99
Lightning NO*	7.1–13.3	7.5–13.9	7.5–13.7	7.3–13.9	7.7–13.9
Total surface CO	1010	1037	1072	1037	985
Isoprene (M)	508 (269)	463 (246)	462 (243)	481 (254)	494 (265)
Isoprene (G)	442 (212)	450 (220)	433 (205)	439 (210)	431 (207)
Monoterpenes (M)	143 (72)	132 (66)	132 (68)	138 (70)	136 (68)
Monoterpenes (G)	35 (11)	36 (12)	34 (11)	35 (11)	34 (11)

M denotes CLM-MEGANv2.1 emissions; G denotes LPJ-GUESS emissions; * Individual model values for the year 2004 are 13.3 (NIWA-UKCA), 12.9 (TM5), 12.4 (GEOS-Chem), and 7.1 (CAM-chem).
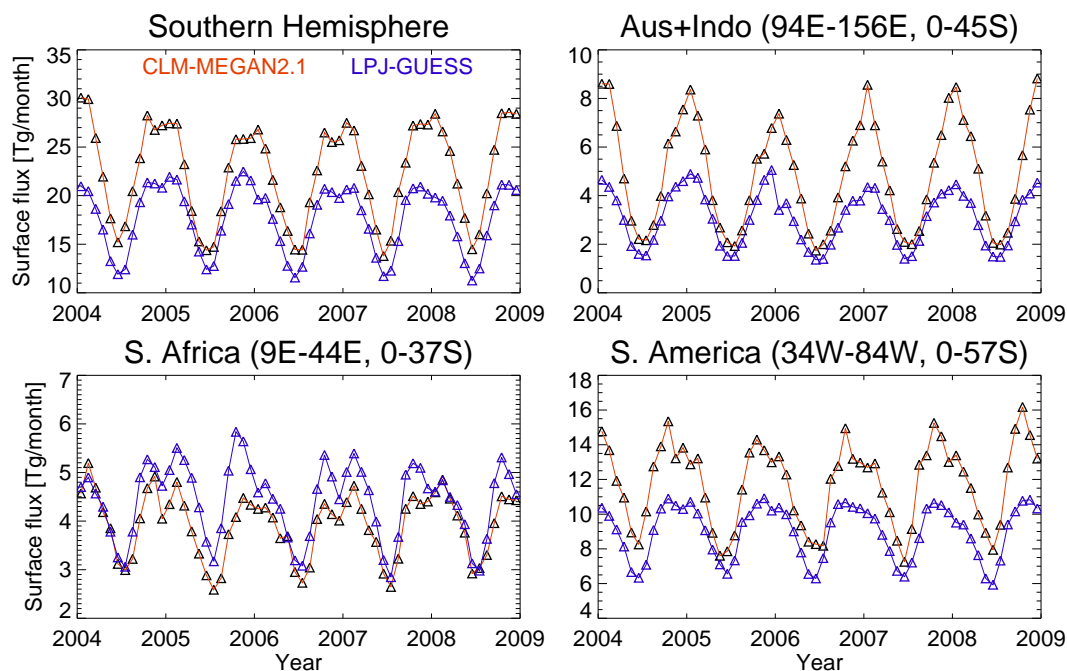
Figure 1. Regional emission fluxes for isoprene between 2004 and 2008 from the CLM-MEGANv2.1 and LPJ-GUESS emission inventories.

cur in austral summer in both data sets when the differences between these two data sets are also largest. Overall, the integrated CLM-MEGANv2.1 isoprene emissions (especially the summer maxima) are substantially higher than LPJ-GUESS emissions with the exception of southern Africa, where LPJ-GUESS emissions are larger. Figure 2 shows the spatial distribution of the fluxes for both isoprene and monoterpenes from the two emission inventories for January 2005. In Amazonia, tropical Africa, and Australia emissions are visibly larger in CLM-MEGANv2.1 than in LPJ-GUESS.

2.2 Models

2.2.1 NIWA-UKCA

NIWA-UKCA stands for the version of the UK Chemistry and Aerosols Model (UKCA) that is used and further developed at the National Institute of Water and Atmospheric Research (NIWA). The background climate model is similar to HADGEM3-A (Hewitt et al., 2011) with a horizontal resolution of $3.75° \times 2.5°$ and 60 vertical levels extending from the surface to 84 km. The physical processes in NIWA-UKCA, including interactive dry and wet deposition of the trace gases and the FAST-JX photolysis scheme, have been described in detail by Morgenstern et al. (2013) and O'Connor et al. (2014). Unlike the version described by O'Connor et al. (2014), here we now apply dry deposition following Wesely (1989) only to the bottom model layer rather than through-
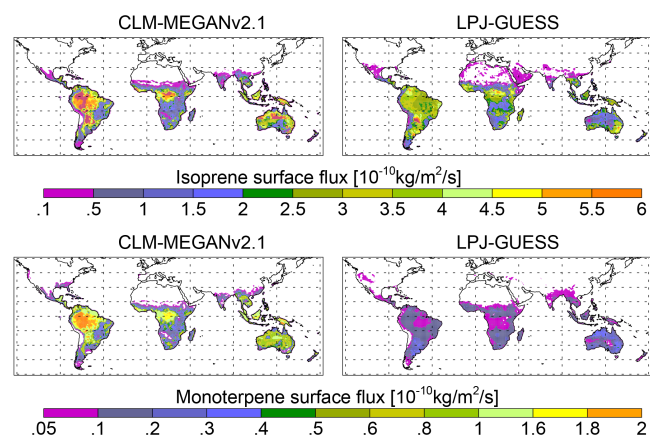
Figure 2. Isoprene and monoterpene emission distributions from CLM-MEGANv2.1 and LPJ-GUESS for January 2005.

out the boundary layer. The model setup used here comprises a coupled stratosphere–troposphere chemistry scheme. The stratospheric reactions are the same as in Morgenstern et al. (2009) and include explicit chlorine and bromine chemistry. We have updated the NIWA-UKCA chemical mechanism from that described in Morgenstern et al. (2013) to account for emissions and degradations of ethene (C_2H_4), propene (C_3H_6), methanol (CH_3OH), isoprene, a representative monoterpene, and a lumped species that accounts for missing NMVOCs in the model similar to the approach taken in the IMAGES model (Müller and Brasseur, 1995), with primary emission sources. In addition to the above, the NIWA-UKCA chemical scheme includes nitrogen oxides (NO_x), CO, ethane (C_2H_6), propane (C_3H_8), HCHO, acetone (CH_3COCH_3), and acetaldehyde (CH_3CHO) as primarily emitted species (O'Connor et al., 2014). The isoprene oxidation scheme is the mechanism described by Pöschl et al. (2000), as previously used by Zeng et al. (2008), but with rate coefficients of reactions between OH and isoprene nitrates and between NO and isoprene peroxy radicals updated following Paulot et al. (2009a, b). A diurnal cycle is imposed on isoprene emissions as a function of the solar zenith angle. We adopt a set of monoterpene oxidation reactions initiated by OH, O_3, and NO_3, described by Brasseur et al. (1998). Methane mixing ratios are prescribed at the surface with a constant value of 1813 ppbv north of the Equator and a constant value of 1707 ppbv south of the Equator, and are the same for each year. Surface emissions are as specified in Sect. 2.1. Lightning-NO emissions are based on the parameterization of Price and Rind (1992, 1994), as a function of convection. The model uses prescribed sea surface conditions following the Atmospheric Model Intercomparison Project (AMIP) II (http://www-pcmdi.llnl.gov). The chemistry is run in a semi-offline mode; i.e. chemistry feedbacks to meteorology and hydrology are deactivated. Table 2 summarizes key model properties for all models.

2.2.2 TM5

TM5 is a global 3-D CTM driven by meteorological fields from the European Centre for Medium-Range Weather Forecast (ECMWF) ERA-interim re-analysis (Dee et al., 2011) using an update frequency of 3 h. Interpolated fields are used for the interstitial time periods. The version used here is identical to that described by Williams et al. (2014) and uses the modified CB05 chemical mechanism (Williams et al., 2013) for describing the chemistry which occurs in the troposphere, along with online photolysis rates. Details relating to the convection, advection, and deposition processes employed are given by Huijnen et al. (2010). TM5 includes a full description of HO_x and NO_x reactions, as well as explicitly treating all C1 to C3 organic species in addition to ammonia (NH_3), sulfur dioxide (SO_2), and dimethyl sulfide (DMS). For this study a horizontal resolution of $3° \times 2°$ is chosen adopting 34 vertical layers from the surface up to 0.5 hPa. The isoprene and monoterpene oxidation schemes are based on the mechanisms developed by Yarwood et al. (2005), with modifications to both the oxidation rate of organic hydroperoxide (ROOH) and the production efficiency of HO_2 from the OH-initiated oxidation of isoprene following recommendations by Archibald et al. (2010). Also in TM5, a diurnal cycle is applied to the monthly mean isoprene emissions. Methane emissions are included and the simulated surface concentrations are then nudged towards a latitudinally and monthly varying climatology based on surface observations; a detailed description of the approach is given by Williams et al. (2013). Mean surface methane mixing ratios for the year 2004 are listed in Table 2, and their interannual variation is small.

2.2.3 GEOS-Chem

The GEOS-Chem global 3-D CTM (www.geos-chem.org) is driven by meteorology from the NASA Global Monitoring and Assimilation Office (GMAO) Goddard Earth Observing System (GEOS-5) assimilated product (Bey et al., 2001). The native GEOS-5 product with $0.667° \times 0.5°$ horizontal resolution and 72 vertical levels (surface to 0.01 hPa) is regridded for computational efficiency to $2.5° \times 2° \times 47$ levels (with all vertical lumping in the stratosphere). Here we use the v9-01-03 coupled O_3–NO_x–HO_x–VOC–aerosol simulation with the Caltech isoprene mechanism (Paulot et al., 2009a, b), which includes 57 transported species (both gas phase and aerosol) and an additional 49 species that interact chemically but are not transported (The detailed chemical mechanism used in this study can be found at http://wiki.seas.harvard.edu/geos-chem/index.php/New_isoprene_scheme_prelim). As monoterpenes are not included as an explicit chemical species, their emissions are used to produce CO (assumed 20 % molar yield; Hatakeyama et al., 1991) and acetone (assume a 12 % molar yield; Jacob et al., 2002). CH_4 mixing ratios are prescribed annu-

Table 2. Summary of model information.

	NIWA-UKCA	TM5	GEOS-Chem*	CAM-chem
Resolution long / lat / lev	3.75°/2.5° / 60	3.0° / 2.0° / 34	2.5° / 2.0° / 47	2.5° / 1.9° / 56
Meteorology	Driven by observed SSTs and sea ice	ERA-Interim	GEOS-5	Specified dynamics, MERRA reanalysis
Mean surface CH_4** (ppbv)	Global 1758, SH 1709	Global 1794, SH 1739	Global 1782, SH 1731	Global 1758, SH 1709
Chemistry	Tropospheric and stratospheric chemistry; 85 species (Morgenstern et al., 2013)	Modified CB05 chemical mechanism, 60 species (Williams et al., 2013)	tropospheric chemistry, 121 species, 106 transported	150 species, MOZART scheme (Emmons et al., 2010)
Isoprene oxidation mechanism	Mainz Isoprene Mechanism (Pöschl et al., 2000) with update OH and NO initiation rates (Paulot et al., 2009a, b)	CB05 (Yarwood et al., 2005); Modified HO_2 yields (Archibald et al., 2010)	Caltech Isoprene Mechanism (Paulot et al., 2009a, b)	MOZART scheme (Emmons et al., 2010)

* GEOS-Chem version v9-01-03 is used in this study.
** Surface CH_4 mixing ratios shown here are for year 2004; NIWA-UKCA uses the same values for each year and the interannual variation is small in other models.

ally and latitudinally based on the National Oceanic and Atmospheric Administration's Global Monitoring Division (NOAA GMD) surface observations and are listed in Table 2. Interactive chemistry is computed in the troposphere only, with stratosphere production and loss rates for most species taken from the NASA Global Modeling Initiative (GMI) Combo CTM Aura4 model (Murray et al., 2013). Stratospheric ozone is simulated using the Linoz linearized ozone scheme (McLinden et al., 2000). Lightning-NO emissions are based on the cloud top height parameterization of Price and Rind (1992) with regional correction to match lightning distributions from satellite, as described by Murray et al. (2012). Other processes in GEOS-Chem v9-01-03 including mixing and deposition are described in detail by Mao et al. (2010, 2013a). The version used here was modified from the standard v9-01-03 to include irreversible HO_2 uptake by aerosols with a gamma value of 0.2 (Mao et al., 2013b), and to include methanol as an interactive tracer based on the off-line simulation of Millet et al. (2008). In the standard GEOS-Chem simulation, biogenic emissions are computed online using a coupled version of the MEGAN model. Here, to ensure consistency with the other SHMIP models, we used the pre-computed biogenic emissions described above (Sect. 2.1) and applied an imposed diurnal variability tied to solar zenith angle.

2.2.4 CAM-chem

CAM-chem is a component of the NCAR Community Earth System Model (CESM). The version used for this study is the same as that used for the Chemistry–Climate Model Initiative (CCMI) (Eyring et al., 2013), and very similar to the CAM4 version described in Tilmes et al. (2015). For SHMIP, CAM-chem was run in the specified-dynamics mode, us-

ing meteorological fields from the Modern-Era Retrospective Analysis For Research And Applications (MERRA) reanalysis product (http://gmao.gsfc.nasa.gov/merra/), regridded to the model horizontal resolution of $1.9° \times 2.5°$, using the lowest 56 levels. In this study, the internally derived meteorological fields (temperature, winds, surface heat, and water fluxes) are nudged at every time step (30 min) by 1 % towards the reanalysis fields (i.e., a 50 h Newtonian relaxation time). The chemical mechanism, based on MOZART-4 (Emmons et al., 2010), includes both tropospheric and stratospheric chemistry, with 150 compounds and 400 photolysis and kinetic reactions, and a tropospheric bulk aerosol model (Lamarque et al., 2012). Heterogeneous reactions on aerosols are included as described in Emmons et al. (2010), including the uptake of HO_2 with a reaction probability of 0.2 producing H_2O_2. While the option of running with online MEGANv2.1 biogenic emissions is available in CAM-chem, this was not used and all surface emissions were based on those specified for this intercomparison, with diurnal variation imposed for isoprene and monoterpenes. Methane surface mixing ratios are specified for monthly zonal averages, as used for CCMI, based on RCP6.0 (Meinshausen et al., 2011). Lightning-NO emissions are determined according to the cloud height parameterization of Price and Rind (1992) and Price et al. (1997). The vertical distribution follows De-Caria et al. (2006) and the strengths of intra-cloud and cloud–ground strikes are assumed equal, as recommended by Ridley et al. (2005).

2.3 Observations of CO and HCHO in the SH

Long-term measurements of trace gases up to the upper troposphere in the remote SH are sparse. Continuous multi-year tropospheric columns of CO are observed at four SH sites:

Darwin, Wollongong, Lauder, and Arrival Heights, with high spectral resolution FTIR spectrometers. In addition, HCHO columns have been retrieved at Wollongong and Lauder. The data records and retrieval methods have largely been presented before (Rinsland et al., 1998, 2002; Jones et al., 2001, 2009; Paton-Walsh et al., 2010; de Laat et al., 2006; Zeng et al., 2012; Morgenstern et al., 2012) and therefore we only give a brief description here.

At Wollongong, Lauder, and Arrival Heights, mid-infrared (MIR) spectra from the FTIR measurements are used to retrieve CO columns, and these stations are part of the Network for the Detection of Atmospheric Composition Change (NDACC; http://www.ndacc.org). The retrieval of trace gas information from these recorded spectra was performed based on the SFIT2 profile retrieval algorithm using the 4.7 µm band, and is similar to that described by Rinsland et al. (1998, 2002). At Arrival Heights, there are no measurements during the polar nights which last 4–5 months per year. CO total columns have been observed at Darwin since 2005 with solar remote sensing using FTIR measurements in the near infrared (NIR), as part of the Total Column Carbon Observing Network (TCCON) (Deutscher et al., 2010; Wunch et al., 2011). The spectra used for CO retrieval are analysed with the GFIT spectral fitting algorithm (Washenfelder et al., 2006) for total column CO. Details of the retrieval method and data are described in Paton-Walsh et al. (2010). Daily averaged time series of CO columns from 2004 to 2008 are used for comparison with the models. Due to the very small "smoothing" error for CO retrievals, which indicates the difference between realistic and retrieved CO columns, averaging kernels are not applied when comparing with the modelled CO data (de Laat et al., 2006; Zeng et al., 2012). Comparisons are made against daily-mean output from each model.

Total columns of HCHO were retrieved at Wollongong and Lauder from the mid-infrared spectra using the SFIT2 inversion algorithm (Jones et al., 2009). HCHO is a very weak absorber in the mid-infrared spectral region. Due to its large "smoothing" errors, the averaging kernels and a priori applied in the retrieval were also applied to the modelled data for a like-with-like comparison between the modelled and retrieved HCHO columns following the method described by Zeng et al. (2012) and references therein.

In order to provide comparisons on a larger spatial scale, we also perform multi-year comparisons for surface CO against flask measurements available from the NOAA Global Monitoring Division network (Novelli et al., 1998). The selected sites are all situated in the SH and cover an extensive latitudinal range. They are typically located away from regions which exhibit strong local emissions of CO. The sites shown are Mahe Island (4.7° S, 55.5° E), Ascension Island (8.0° S, 14.4° W), Pacific Ocean (30.0° S, 176.0° W), Baring Head (41.4° S, 174.9° E), Crozet Island (46.4° S, 51.9° E), Tierra del Fuego (54.9° S, 68.3° W), Syowa Station (69.0° S, 39.6° E), and South Pole (90° S, 24.8° W). The locations of
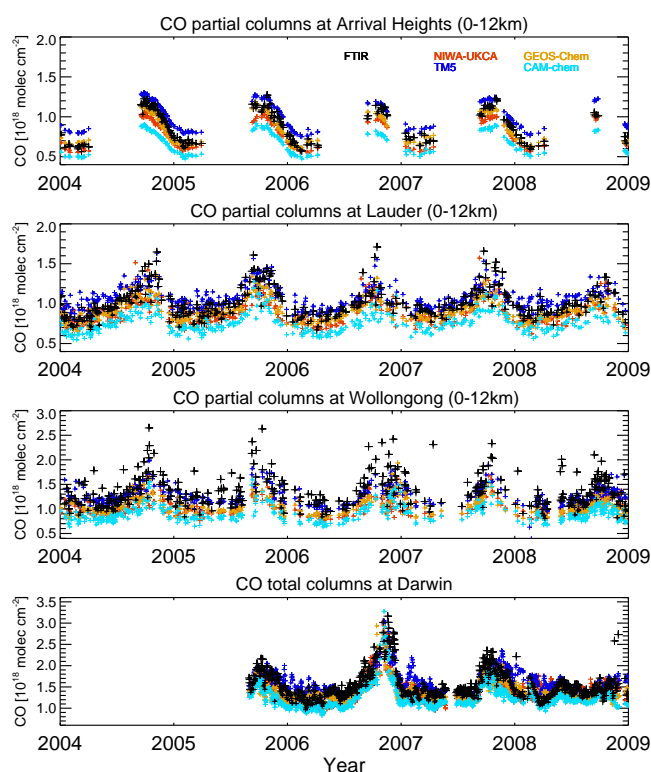

Figure 3. Modelled and observed daily-mean FTIR CO columns at SH stations from four models. Simulations use CLM-MEGANv2.1 biogenic emissions.

all sites used in this study are displayed in Fig. S1 in the Supplement.

To illustrate how the models perform on the global scale in general, we also show comparisons between modelled CO and observed CO columns made by the Measurements Of Pollution in the Troposphere (MOPITT) satellite instrument (https://www2.acd.ucar.edu/mopitt). We use the MOPITT version 6 level 3 thermal-infrared product, and the data are monthly averages. A description of the data and the retrieval method is given by Deeter et al. (2003, 2014). Here the daytime monthly mean MOPITT CO columns for January and September 2005 are used for comparison. Model outputs are monthly averaged and have been interpolated to the MOPITT horizontal grid of 1° × 1° and 10 vertical levels with a 100 hPa spacing. The MOPITT CO averaging kernel and a priori data are applied to the calculation of the modelled CO columns, as described by Morgenstern et al. (2012) and the references therein; such an approach is generally recommended when comparing modelled data to data from satellite remote-sensing instruments (Rodgers et al., 2003).

3 Comparison between models and observations

3.1 FTIR CO columns

Figure 3 shows the direct comparison between modelled and FTIR daily-mean CO columns for the CLM-MEGANv2.1 simulation. Here, we use the tropospheric FTIR partial columns, for the reasons that not all models have well-resolved stratospheric chemistry in the model, there is a significant contribution of CO from the mesosphere during polar spring (Velazco et al., 2007), and that all models lack or have deficiencies in handling the mesospheric chemistry. FTIR CO partial columns (0–12 km) are used for comparison at Arrival Heights, Lauder, and Wollongong instead of total columns. However, the partial columns of CO at Darwin are not available so we use total columns for comparison. Note that the contribution of mesospheric CO to the total column is expected to be minimal at Darwin given its tropical location (Velazco et al., 2007); therefore, the differences between the partial and the total columns are expected to be small. The model data at all locations have been interpolated to the dates when the measurements were carried out. Figure 3 shows that CO seasonal cycles are well reproduced by all four models at all locations. Models accurately reproduce the total columns of CO at Darwin with very small inter-model differences. The Darwin measurement site is the closest to the tropical source regions; this indicates that the emissions in this area are well represented in the models. Inter-model differences are notably larger at other sites which are located further from the source regions, with consistent overestimation by TM5 and underestimation by CAM-chem at both Arrival Heights and Lauder. Such differences are possibly associated with both differences in the oxidative capacities in these two models and differences in transport (discussed in Sect. 4). All models underestimate CO columns at Wollongong, especially during the peak BB season; this may be due to its proximity to large forested areas and/or the cities of Sydney and Wollongong whose direct emissions may be underestimated in the MACCity inventory. Note that due to the coastal location of Wollongong, model grid boxes may not be representative of the measurement site.

We performed a second set of simulations using LPJ-GUESS isoprene and monoterpene emissions (see Fig. S2 in the Supplement); the models visibly underestimate the observed FTIR tropospheric CO columns at all sites. The deviation of model ensemble-mean CO columns from the observed FTIR columns are shown at the four measurement sites (Fig. 4) in comparison with the simulation using CLM-MEGANv2.1 biogenic emissions. The differences between these two simulations are also shown (i.e. CLM-MEGANv2.1 minus LPJ-GUESS). It appears that a larger negative bias exists when adopting the LPJ-GUESS emissions for all of the column measurement stations (i.e. CLM-MEGANv2.1 results in better agreement with the FTIR observations). The deviations of both simulations from the ob-
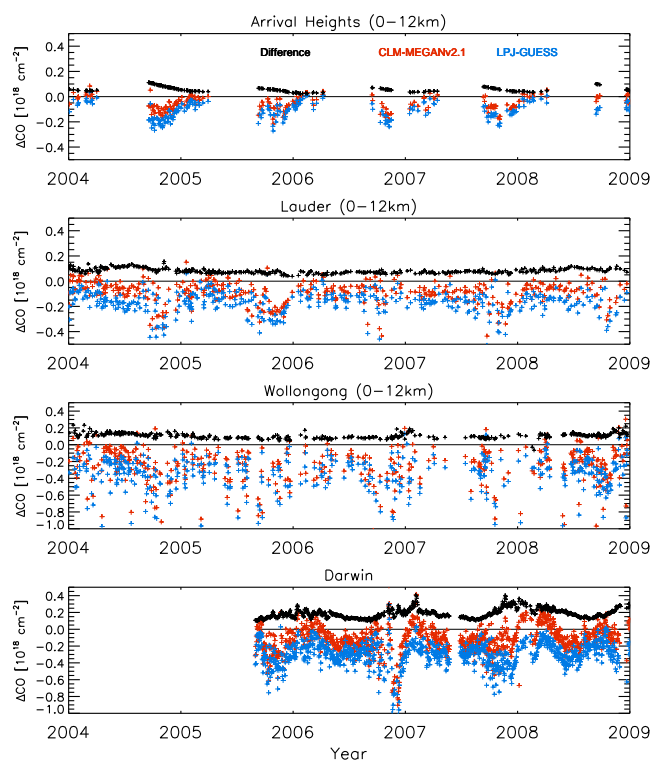

Figure 4. Deviations of model ensemble- and daily-mean CO columns from the observed FTIR CO columns with CLM-MEGANv2.1 simulation (red) and with LPJ-GUESS simulation (blue) respectively. The difference between the modelled CO columns from these two simulations are displayed in black symbols ($CO_{CLM\text{-}MEGANv2.1} - CO_{LPJ\text{-}GUESS}$).

Table 3. Multi-annual averaged ensemble model mean deviations (%) from observed FTIR CO columns.

	CLM-MEGANv2.1	LPJ-GUESS
Arrival Heights	−3.2 %	−10.5 %
Lauder	−8.6 %	−17.1 %
Wollongong	−19.2 %	−27.5 %
Darwin	−6.9 %	−19.9 %

served CO columns exhibit large seasonal variations but seasonal and interannual variations are consistent between these two simulations.

Figure 5 shows differences between the modelled and observed FTIR CO columns at the four measurement sites from the multi-annual ensemble-mean data for both CLM-MEGANv2.1 and LPJ-GUESS simulations. As in Fig. 4, the seasonal variations of the biases from these two sets of simulations follow a very similar pattern, implying that the effect of different biogenic emissions is reflected in the differences in the background CO columns in the SH. The biases shown in the ensemble model means from both simulations are largest during the SH tropical BB season of September,
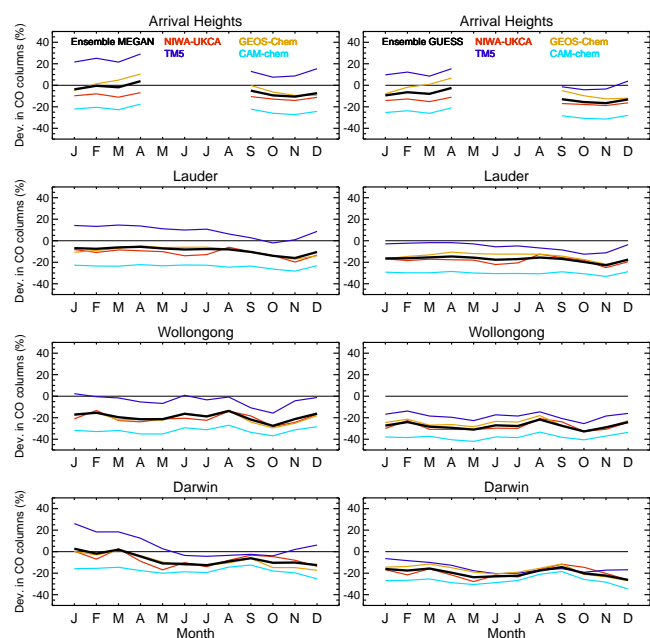
Figure 5. Percentage differences between modelled and observed multi-annual mean CO columns at Arrival Heights, Lauder, Wollongong, and Darwin from two simulations with CLM-MEGANv2.1 (left) and LPJ-GUESS emissions (right) respectively.
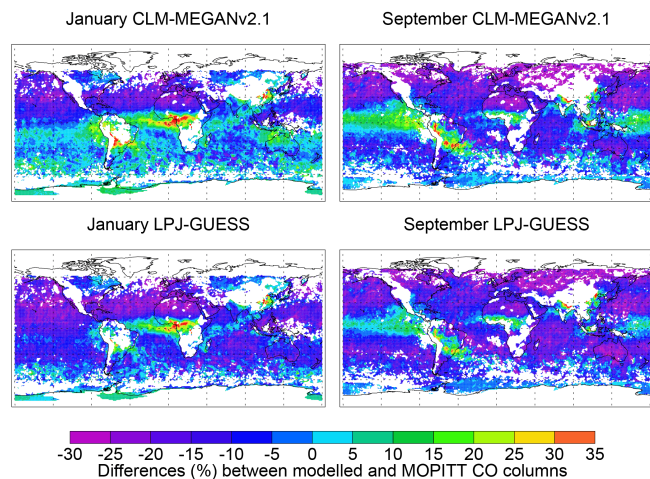

Figure 6. Percentage differences between ensemble model mean and MOPITT CO columns for January and September 2005, from two simulations with CLM-MEGANv2.1 (top) and LPJ-GUESS (bottom) biogenic emissions, respectively.

October, and November (SON), although at Darwin the negative biases are also high in July and increase from October to December. For Wollongong, Lauder, and Arrival Heights the largest negative biases are in October, November, and December, respectively; this suggests an underestimation of SH BB sources in GFEDv3 and the subsequent effect on CO columns at SH remote locations through long-range transport. At Darwin, CO columns are more likely influenced by

local or nearby BB sources which may have a different seasonality. The annually averaged biases of the model ensemble means for each site are shown in Table 3; the lowest biases are at Arrival Heights for both simulations, followed by those for Darwin, Lauder, and Wollongong. Note that the low ensemble bias at Arrival Heights is largely the result of cancellation of a positive bias in TM5 with a negative bias from CAM-chem with a similar magnitude. The large spread between the models indicates that substantial differences exist in other physical and/or chemical processes which are unrelated to emissions.

The individual model biases are also shown in Fig. 5. For both simulations, inter-model variability is notably larger during months that lie outside the seasons when most intensive BB occurs, i.e. typically in austral summer and autumn (covering December and January to May). Such a seasonal dependence of inter-model variability is consistent with that described by Fisher et al. (2015) who compare modelled vertical CO gradients in the Cape Grim region using the same simulations, and is due to the difference in chemistry that controls CO chemical production and loss processes in the seasons other than the peak biomass burning season. Inter-model variability is generally larger in CLM-MEGANv2.1 than in LPJ-GUESS for all seasons and locations, primarily due to the larger response of modelled CO to its higher precursor emissions.

3.2 MOPITT CO columns

MOPITT CO columns and the individual model biases for January and September 2005 are shown in Fig. S3 in the Supplement. The model data are monthly means convolved with the MOPITT averaging kernels and a priori data. MOPITT data exhibit a lot of gaps over the Amazon region in January and over Africa in September, due to persistent cloud cover. All models underestimate MOPITT CO columns in the NH (with the exception of East Asia), and overestimate CO in the plumes, particularly over the tropical Atlantic in January and the Pacific in September. These plumes originate in tropical Africa and South America, respectively, indicating an overestimation of biomass burning emissions in these regions. Comparing the models, TM5 shows higher CO columns throughout the SH and CAM-chem the lowest, in agreement with the comparison of FTIR CO columns. Figure 6 shows the percentage differences between the ensemble-mean modelled and measured columns for both the CLM-MEGANv2.1 and the LPJ-GUESS simulations. There is a general underestimation of CO columns by both ensembles in the NH by up to $\sim -25\%$. Both ensembles overestimate CO in the source regions, with up to $+30\%$ over tropical Africa in January and over Amazonia in September, i.e. during the months of peak biomass burning. In the SH, away from the CO plumes, the CLM-MEGANv2.1 ensemble clearly compares better with MOPITT CO than the LPJ-GUESS ensemble, with biases typically between -10 and $+10\%$ in January and Septem-
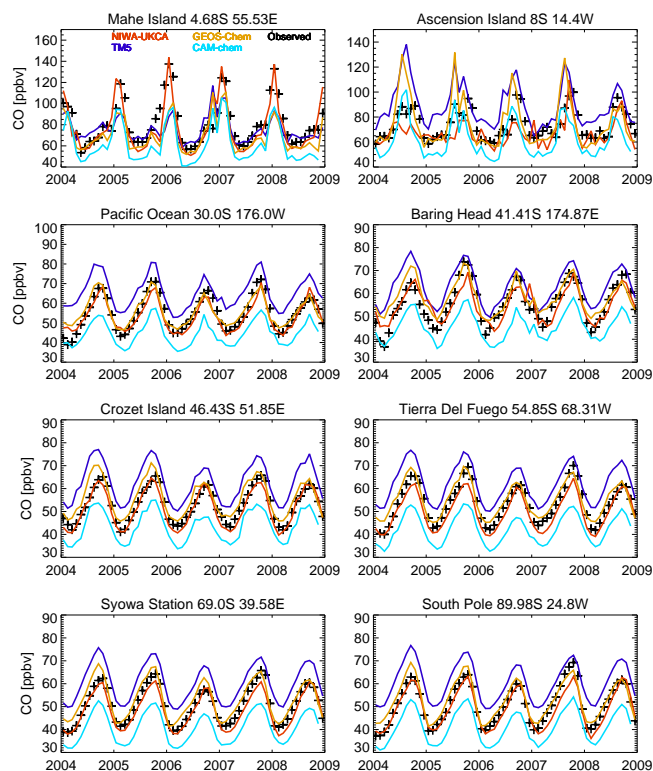
Figure 7. Modelled monthly mean surface CO with CLM-MEGANv2.1 emissions (coloured lines) and observed monthly mean surface CO at SH sites. Observations are from the NOAA GMD network (Novelli et al., 1998): http://www.esrl.noaa.gov/gmd/.

ber, whereas errors typically are in the range −20 to −5 % from the LPJ-GUESS ensemble. Both ensembles also underestimate CO columns over Australia in September, which suggests an underestimation of biomass burning in GFEDv3. This is also reflected in the comparison between modelled and FTIR CO columns in the four SH locations shown above, which generally show negative biases in modelled CO. The two ensembles are fairly similar in the NH with regard to their CO columns but exhibit significant differences in the extratropical SH. This is consistent with a larger relative role of biogenic emissions in the SH versus the NH.

3.3 Surface CO

To assess the models' ability to capture both the seasonality and interannual variability of CO at the surface over the simulation period, we show in Fig. 7 comparisons between the CLM-MEGANv2.1 simulations and monthly mean CO values observed at the eight surface sites listed in Sect. 2.3. Consistent with the FTIR column comparisons, all models capture the seasonal cycles of observed surface CO at each location. In line with Fig. 3 in Fisher et al. (2015), TM5 typically exhibits a high bias and CAM-chem exhibits a low bias of the order of 5–10 ppbv. Large variations exist in seasonal

cycles at both Mahe Island and Ascension Island, but the timing of the peaks are different. At Mahe Island, surface CO peaks in January and February due to the influence of anthropogenic emissions from India (Wai et al., 2014), whereas at Ascension Island, the seasonal cycle is principally driven by CO which originates from BB in southern Africa during June–July–August (e.g. Williams et al., 2012; Wai et al., 2014). The interannual variability and timing in peak mixing ratios is not captured well at Ascension Island, especially for GEOS-Chem and TM5; this is possibly related to too strong westerly transport out of southern Africa and too weak an oxidative capacity, especially in TM5. For the more southerly oceanic sites, the seasonal cycles and amplitudes are remarkably similar, indicating that the variability in background CO is rather low at the surface in the SH remote locations. In general, NIWA-UKCA and GEOS-Chem display a better agreement with the observations in the remote SH, indicating that their oxidative capacities are more realistic. The consistent high and low biases in TM5 and CAM-chem, respectively, are related to the oxidizing capacity in these models; this is discussed in Sect. 4.

We quantify the differences between the multi-annual ensemble means for surface CO and the corresponding values derived from the observations for both the CLM-MEGANv2.1 and the LPJ-GUESS simulations (Fig. 8). As was seen in the model comparisons to the FTIR and MO-PITT CO data, the observed distributions of surface CO in the SH are better reproduced by CLM-MEGANv2.1 for most of the chosen sites. A comparison of sites shows that the seasonal biases are more variable for the tropical sites which are affected by the interannual variability in tropical BB. For the mid- to high-latitude sites, the CLM-MEGANv2.1 ensemble mean accurately reproduces the observations in most cases, whereas the LPJ-GUESS ensemble is consistently biased low. The individual model biases (shown only for the CLM-MEGANv2.1 simulation) are up to ±20 %, and are much larger than the differences between the two ensemble means (~10 %). The generally better agreement between modelled and observed surface CO, relative to the agreement between modelled and FTIR CO columns in the remote SH, reflects that there may be some deficiencies in the models' vertical transport of either CO and/or its precursors. This generally underestimation of observed vertical gradients of CO by the models in the remote SH was shown by Fisher et al. (2015) for the Cape Grim region.

3.4 HCHO columns

Here we examine the models' ability to reproduce observed HCHO columns at the SH mid-latitude sites Lauder and Wollongong. Figure 9 shows comparisons between modelled daily-mean HCHO columns (from the CLM-MEGANv2.1 simulation) convolved with FTIR a priori data and averaging kernels, and observed daily-mean HCHO columns from the FTIR measurements. The seasonal cycles are generally well
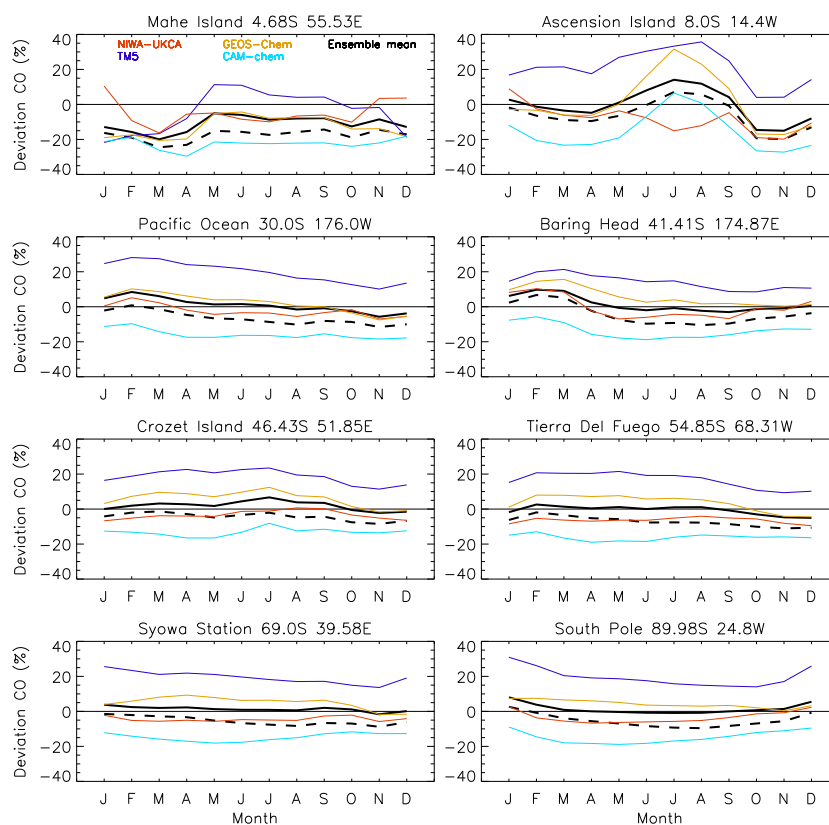
Figure 8. Percentage differences between monthly mean modelled and observed surface CO; solid black lines for CLM-MEGANv2.1 ensemble and dashed black lines for LPJ-GUESS ensemble. Individual model deviations (coloured lines) are from the CLM-MEGANv2.1 simulations only. Data are averaged over 2004–2008.
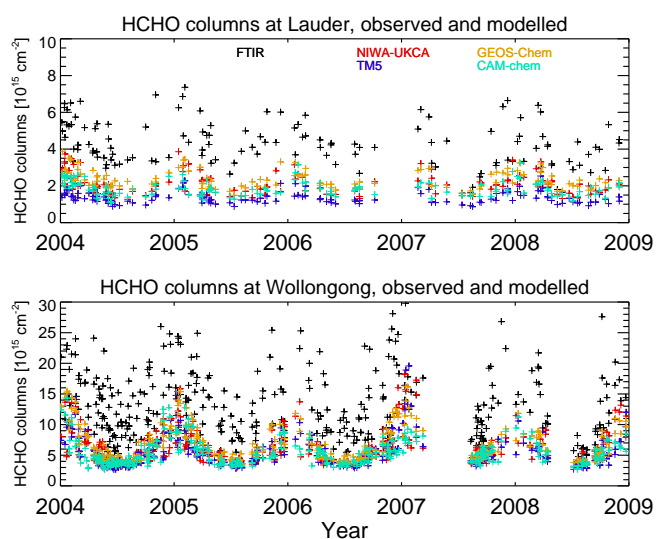

Figure 9. Modelled and observed daily-mean FTIR HCHO columns at Lauder and Wollongong. Simulations use CLM-MEGANv2.1 biogenic emissions.

reproduced across the entire model ensemble, with the seasonal maxima in austral summer and the minima in winter, but all models significantly underestimate observed columns in all seasons. Inter-model differences in modelled HCHO columns are larger at Lauder than at Wollongong; the highest HCHO columns are produced in GEOS-Chem, whereas the lowest are from TM5. Such variations between the models indicate that the differences in the models' chemistry are the driving factor, in particular at the sites that are further away from the emission sources. Significant and persistent low bias across all models cannot be reconciled by considering the diurnal cycle in HCHO; for testing purposes, we also calculated HCHO columns by replacing daily-mean HCHO data shown in Fig. 9 with the daily maximum of the 3 hourly data from one of the ensemble members (CAM-chem). This resulted in small overall changes, with ∼ 10–15 % increases that occur in some summer months, and the increases were not sufficient to close the gap between the models and the observations. Therefore, we are confident that using daily-mean modelled HCHO columns for comparing to columns from FTIR observations that occur during the daylight is satisfactory. Figure 10 shows the multi-annual monthly mean FTIR HCHO columns and model ensemble means averaged
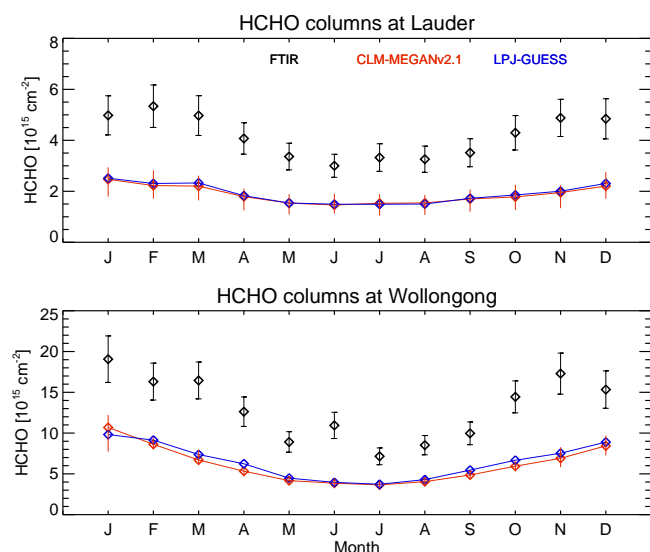
Figure 10. Observed (black symbols) FTIR multi-annual monthly-mean HCHO columns and corresponding multi-model mean from CLM-MEGANv2.1 (red) and LPJ-GUESS (blue) simulations. Measurement errors are shown by vertical bars (black). Model ranges from the CLM-MEGANv2.1 simulations are also given (coloured vertical bars).

for the same years with both CLM-MEGANv2.1 and LPJ-GUESS emissions for isoprene and monoterpenes. Overall, the models underestimate the observed HCHO columns by approximately 50 %. Differences in biogenic emissions do not appreciably affect this.

In the case of Wollongong, proximity to Sydney and the influence of episodic BB events in the vicinity (Williamson et al., 2013) could introduce local direct and indirect sources of HCHO and chemical precursors which are unaccounted for and might have contributed to the low bias simulated in the models, particularly for the seasonal peaks. However, at Lauder there are no known significant local sources of HCHO. We therefore assume that the underestimation of observed FTIR HCHO columns by the models is very likely related to missing emissions of precursors.

The underestimation of measured HCHO by the models at the remote SH locations had been shown in some previous studies, and in those studies various assumptions about missing processes have been explored (e.g. Ayers et al., 1997; Jones et al., 2009; Vigouroux et al., 2009). Ayers et al. (1997) used a box model to simulate the measured surface HCHO at Cape Grim and were unable to capture the magnitude of the observed mixing ratios of HCHO by including a set of standard methane oxidation reactions in the model. Among the major HCHO production channels, Ayers et al. (1997) assumed a 100 % yield of CH_3OOH from $CH_3O_2 + HO_2$. Ayers et al. (1997) then experimented with an alternative oxidation pathway that involved the direct production of HCHO (40 %) from $CH_3O_2 + HO_2$, which resulted in a much im-

proved comparison. We have not applied such high direct yield of HCHO in our models. However, following the recent recommendation of the International Union of Pure and Applied Chemistry (IUPAC) (Atkinson et al., 2006), a 10 % direct yield of HCHO has been adopted by NIWA-UKCA but no direct yield has been applied in the other three models. The recent IUPAC recommendations (Atkinson et al., 2006) assume a temperature-dependent branching ratio for the direct HCHO production channel (i.e. 0.09 to 0.29 for temperatures ranging from 298 to 218 K). Adopting this recommendation, an additional test was performed in TM5, showing some modest increases in HCHO in the extratropics of up to ∼ 10 %. However, this is not sufficient to explain the large bias shown here. Another hypothesis suggested by Ayers et al. (1997) is the possibility of a small marine biological source of isoprene (e.g. Bonsang et al., 1992). Recently, Lawson et al. (2015) found relatively abundant HCHO precursors (dicarbonyls) in two regions of the southwest Pacific, corroborating the hypothesis that marine biological activity might be responsible for the measured HCHO abundance. However, spatial sampling and understanding of the underlying biological processes remain poor.

The HCHO column data set we use here is an extension of the 1992–2005 data set described by Jones et al. (2009), retrieved using the same algorithm. They also derived HCHO mixing ratios at a coarse vertical resolution. Jones et al. (2009) performed a box model simulation based on subsets of the Master Chemical Mechanism (MCM) (Saunders et al., 2003) including the isoprene oxidation scheme of the MCM. They found that high-HCHO mixing ratios retrieved at Lauder cannot be explained by methane oxidation alone and that additional local sources, possibly isoprene, are needed to explain the observed near-surface HCHO mixing ratios at Lauder. A recent study by Vigouroux et al. (2009) compared modelled and observed FTIR HCHO columns at Réunion Island, using the global chemical transport model IMAGESv2; they also underestimate the observed FTIR HCHO columns albeit with a smaller magnitude than that shown in this study. The time series shown by Vigouroux et al. (2009) are for August to November 2004 and for May to November 2007, respectively, and the differences between modelled and observed HCHO columns are around 30 and 25 %, respectively. The isoprene mechanism used by Vigouroux et al. (2009) is based on the MCM and is described by (Müller and Stavrakou, 2005). The isoprene emissions used by Vigouroux et al. (2009) are from the MEGAN-ECMWF inventory (Müller et al., 2008), and the yearly totals averaged over 2004 to 2006 are around 10 % lower than the CLM-MEGANv2.1 inventory used here. To investigate the possible causes for the low bias in modelled HCHO, Vigouroux et al. (2009) include methane oxidation by tropospheric chlorine, but the impact of this process on HCHO columns is only about 1–2 % and therefore cannot explain the underestimation. They also experimented using a different OH climatology; this increase of OH abundance results
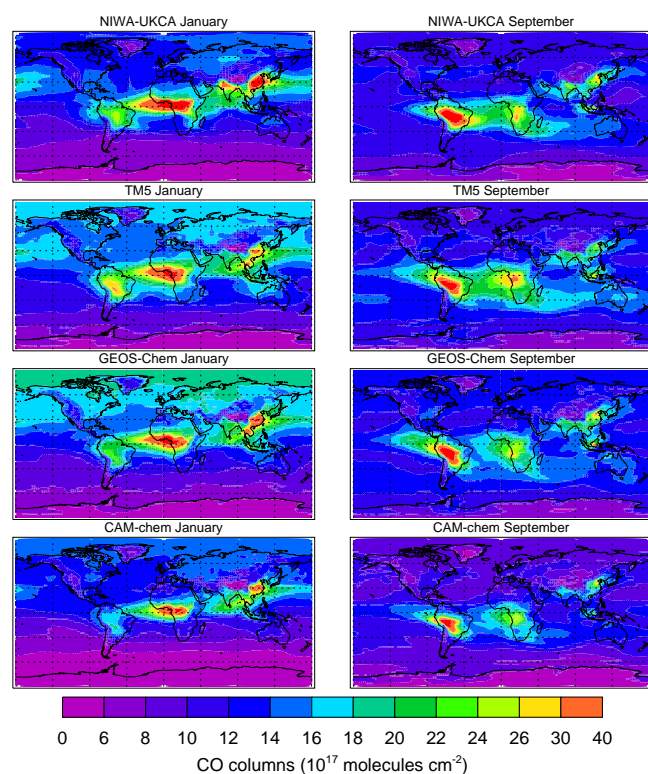
Figure 11. Tropospheric CO columns from the four models for January (left) and September (right) 2005, for the CLM-MEGANv2.1 simulations.

Figure 12. Tropospheric CO_{25} tracer columns from four models for January (left) and September (right) 2005, for the CLM-MEGANv2.1 simulations.

in better agreement between observed and modelled HCHO columns but cannot fully reconcile the substantial differences, and a more probable explanation is an underestimation of HCHO precursors transported from Madagascar to Réunion Island. This finding, together with our finding here, suggests that the underestimation of HCHO columns is persistent throughout the SH. Observations of HCHO in the remote SH regions are extremely sparse, and it is impossible to fully constrain modelled HCHO. Note that in both studies (Jones et al., 2009; Vigouroux et al., 2009), FTIR HCHO columns compare well with satellite measurements, and with both satellite and MAX-DOAS measurements, respectively. This again suggests that the FTIR HCHO retrieval is robust at all sites, and that the likely cause for model-observation differences is missing sources of HCHO and/or its precursors in the models.

4 Model differences in chemistry and transport

Although the four models are constrained by the same emissions, there are significant differences in the models' abilities to reproduce observed CO columns and surface CO in the remote SH, as shown above. Here we explore the underlying factors driving these differences. To diagnose the extent of differences in transport between the models, we ex-
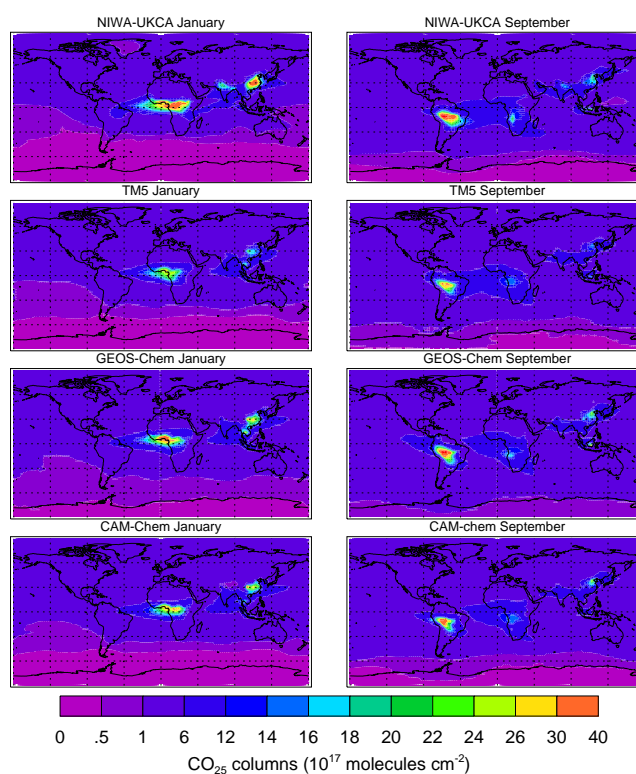
amine the two passive CO tracers defined in Sect. 2: one with a fixed lifetime of 25 days (referred to as CO_{25}) and the second with first-order loss via model calculated OH (referred to as CO_{OH}). Both tracers are subjected to the same surface emissions as the full simulations, but not subjected to any secondary production of CO from methane and NMVOC oxidation. Dry deposition of CO is not included for either of the additional CO tracers as it is considered a minor loss channel for the SH.

The global tropospheric CO columns from all models for January and September are shown in Fig. 11. January and September represent the seasonal maxima of biogenic and biomass burning emissions in the SH, respectively. Here, we define the tropospheric columns as the columns below the chemical tropopause marked by the 150 ppbv O_3 isopleth in each model (monthly mean O_3 used here is averaged over 2004–2008). Although here we focus on the SH, we note that the inter-model differences apparent in the SH are consistent with those occurring in the NH, namely, the lowest CO columns occur in CAM-chem, followed by NIWA-UKCA, with higher CO columns from GEOS-Chem and TM5 for both hemispheres, indicating systematic differences between the models. Comparing the seasonal variations, CO columns are generally higher in September than in January in the SH, primarily due to the timing of the most intensive tropical BB

events in austral spring. Of the four models, CAM-chem simulates the lowest CO columns in both the source regions and in the remote mid- to high latitudes. Examining the distributions of the tropospheric columns of CO_{25} shown in Fig. 12, CO_{25} exhibits similar distributions among the models for both seasons in source regions as those shown in Fig. 11. The differences become more obvious in the extratropics, with NIWA-UKCA showing slightly weaker transport towards the poles, whereas GEOS-Chem shows somewhat stronger export of CO_{25} out of the source regions and towards the poles. Overall, despite some differences, the magnitude and distribution of CO_{25} are very similar among the models. However, such differences and similarities in transport among the models are not reflected in the differences in CO columns shown in Fig. 11 in which TM5 simulates the highest CO columns and CAM-chem the lowest in both the source and remote regions. CO_{OH} (Fig. S4 in the Supplement) is a more realistic proxy of CO, reflecting the influences of the models' variable OH concentrations. Like CO_{25}, the magnitudes and distributions of CO_{OH} are similar across the models; hence, the main driver of the model differences in total CO cannot be attributed to primary emissions.

Next, we quantify the roles of transport and chemistry in determining the inter-model variability in CO columns in the SH. We examine three zonal bands defined as 0–30, 30–60, and 60–90° S. These latitude bands capture the main tropical source regions and mid- and high latitudes, respectively. Figure 13 shows the monthly mean tropospheric columns of CO as well as ratios of CO_{25}/CO and CO_{OH}/CO columns, averaged across each of these zones for each model. $CO_{sec} = CO - CO_{OH}$ is an estimate of the fraction of CO that is produced by oxidation of CH_4 and NMVOCs; the ratio of CO_{sec} to CO is also shown in Fig. 13. These ratios define the contributions of CO_{25}, CO_{OH}, and CO_{sec} to the total CO columns in each model. Figure 13 shows that CO columns decrease towards the high latitudes and the seasonal maxima are during the September/October BB season in all zones. Although CO_{25} is an idealized tracer designed to diagnose differences in the long-range transport simulated in each model, CO_{OH} should be a more realistic measure of how much primary emissions of CO contribute to the CO columns because CO_{OH} reflects the locally varying lifetime of CO due to the spatial variability of OH. The ratio of CO_{25} to CO drops sharply from the tropics to the pole for all models (from ~ 20 to ~ 5 % in the annual average), as would be expected from the hemispheric distribution of emissions and the timescales for meridional transport. By contrast CO_{OH}/CO reduces only from ~ 30 to ~ 25 % in the yearly average. This reflects that the lifetime of CO is considerably longer outside of the source region due to lower background O_3 levels (and therefore lower OH levels) in the more pristine environment away from strong NO_x sources. CO_{sec}/CO shows a moderate increase from 70 to 75 % from the tropical zone to the high latitudes. Overall, primarily emitted CO makes up ~ 25–45 % of total tropospheric CO in

the source region and ~ 20–40 % in the polar region, depending on season, while the secondary CO makes up the remainder of the tropospheric columns, i.e. ~ 55–75 % in the source region and ~ 60–80 % in the polar region. Regarding seasonal variability, CO_{25} and CO_{OH} have proportionally larger contributions in austral spring when BB dominates the CO emissions, whereas CO_{sec} shows larger contributions in austral summer/autumn. Of all the models, NIWA-UKCA shows the smallest contribution from primary CO to the columns and the largest contribution from the secondary CO, relative to the other three models.

Inter-model differences in CO columns and the additional CO tracers are expressed as the ratio of individual model columns vs. the multi-model mean columns for each zone, shown in Fig. 14. For CO columns, the inter-model differences are smallest in the tropical zone and gradually increase towards the pole, with the highest CO columns from TM5 and the lowest from CAM-chem, in agreement with the FTIR comparisons and the surface comparisons shown earlier. Examining the inter-model differences in CO_{25}, the model spread increases substantially towards the polar zone, and is characterized by the strongest transport out of the source region from GEOS-Chem and the weakest from NIWA-UKCA (also shown in Fig. 12). Note that this behaviour is not reflected in the model spread of CO columns (i.e. the highest CO occurs in TM5 and the lowest in CAM-chem). By contrast, the patterns of model spread in CO_{sec} and to a lesser degree in CO_{OH} are consistent with that seen in the CO columns, indicating that the inter-model differences in modelled CO columns are strongly influenced by the differences in CO_{sec}, which is dependent on the oxidizing capacity in the model that also drives the loss of primary-emitted CO by OH. Considering also the absolute contributions of both primary CO sources and secondary CO production to the SH CO columns (these being ~ 35 and ~ 65 %, respectively), we can deduce that inter-model differences in CO columns attribute about one-third to primary and two-thirds to the secondary CO production in the SH. Note that here we only take into account the accumulated effects of primary and secondary contributions to CO; we do not differentiate or individually identify the separate influences, e.g. of transport and chemistry. For example, the large CO columns in TM5 can be the result of combined effects of slower chemical loss of CO due to lower OH levels in the model and a faster secondary CO production in the source region, as reflected in higher ratios of CO_{sec} to CO shown in Fig. 15. In contrast, GEOS-Chem CO has faster loss by OH than TM5 (but slower than the others), but this is outweighed by a stronger transport resulting in higher CO compared to that in NIWA-UKCA and in CAM-chem. For CAM-chem, moderately slow transport of CO out of the source region combined with slower secondary CO production results in the lowest CO columns. More quantitative analyses of differences in chemistry are carried out in Sect. 5.
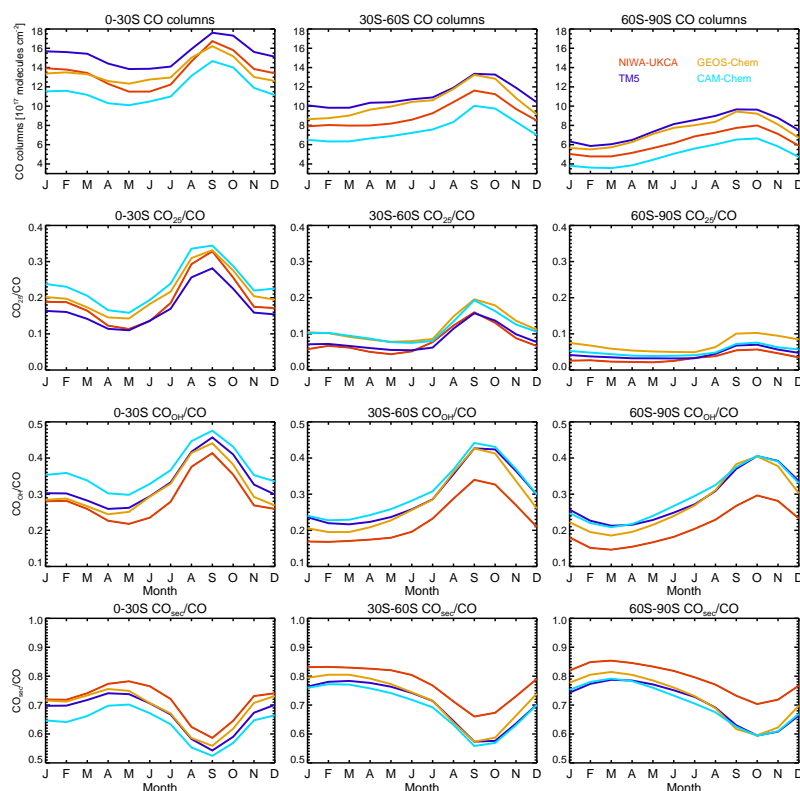
Figure 13. Monthly mean CO columns (top) and the ratio of CO_{25} to CO, CO_{OH} to CO, and CO_{sec} to CO columns averaged over three SH regions (0–30, 30–60, and 60–90° S). Data are for the year 2005.

To further probe the differences between the models, we show vertical profiles of modelled key species, namely CO, HCHO, O_3, and OH mixing ratios from each model in Fig. 15. We display data for January 2005 from the CLM-MEGANv2.1 simulation, because in austral summer the chemical production maximizes due to stronger photochemistry and higher biogenic emissions, and absolute inter-model differences in CO columns are also larger than in other seasons. TM5 is characterized by consistently high CO throughout the SH. The CO values in NIWA-UKCA and in GEOS-Chem are very close in all three zones, exhibiting differences of ~ 5–$10\,\%$, although CO in NIWA-UKCA is slightly higher than that in GEOS-Chem in the tropics but becomes lower towards remote regions. This may reflect slower meridional transport in NIWA-UKCA (shown in CO_{25}) combined with larger chemical production in the source region. The HCHO mixing ratios decrease sharply with altitude due to the dominant chemical precursors residing in the boundary layer and the efficient photo-dissociation, but the vertical gradient becomes smaller away from the source region, particularly in TM5, due to depletion of the biogenic precursor emissions in the remote SH. HCHO abundances in the four models correlate with OH to some extent; i.e. both OH and HCHO are relatively large in GEOS-Chem, whereas both are relatively small in TM5; this reflects the approximate linear-

ity between the modelled HCHO abundance and methane oxidation via OH in the remote SH. However, there is no simple linear relationship between HCHO and OH; OH is involved in both the loss and the production of HCHO, and HCHO is one of the OH sources. The modelled OH profiles do not seem to be closely related to O_3 (the primary source of OH) in that TM5 has the lowest OH but its O_3 values lie in the middle of the model range; this is likely due to differences in photolysis schemes. Water vapour fields are very similar among the models.

5 Analysis of chemical production and loss rates

To quantify the effects of differences in model chemistry, we analyse chemical production (CP) and chemical loss (CL) rates of CO and of HCHO, as listed in Tables 4 and 5 for both simulations (i.e. with CLM-MEGANv2.1 and LPJ-GUESS emissions, respectively). The budget terms displayed are for year 2004 and for the whole globe, the SH, and the three SH latitudinal bands defined above. The corresponding burdens of CO, HCHO, and OH are shown in Table 6. We define the tropopause of each model as the 150 ppbv O_3 isopleth in each model, as in Sect. 4.

Examining the CO budget terms shown in Table 4, the SH CPs and CLs of CO are under half of the global values. The
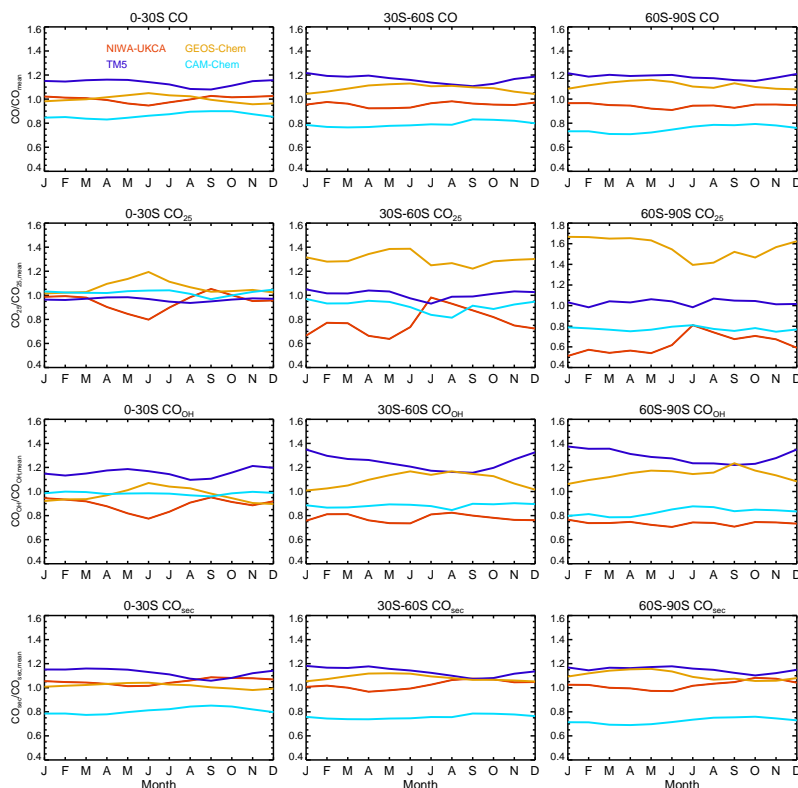
Figure 14. The ratio of individual models to the ensemble-mean columns averaged over three SH regions (0–30, 30–60, and 60–90° S) for CO, CO_{25}, CO_{OH}, and CO_{sec}. Data are for the year 2005.

main contribution to the SH CPs come from the 0–30° S latitude band; production decreases sharply towards the southern polar region. In general, chemical production and loss rates of CO are larger in the CLM-MEGANv2.1 simulations, indicating larger biogenic emissions leading to larger CO production. However, the CO production from methane oxidation is generally larger in LPJ-GUESS as a result of increased OH (shown in Table 6) due to the reduction of biogenic emissions. In all models, the ratio of CP of CO to surface emissions is markedly larger in the SH than the global values; this results in larger inter-model differences in the SH due to the differences in the models' underlying chemistry. NIWA-UKCA shows the largest total CPs for all domains, followed by GEOS-Chem, TM5, and CAM-chem, and the differences in total CPs are dominated by the differences in the oxidation of NMVOCs. Methane oxidation is more constrained among the models, and the differences in methane oxidation are mainly driven by differences in OH (shown in Table 6). Note that we do not calculate CO production rates from NMVOC oxidation explicitly in the models; instead they are deduced from the total CP and methane oxidation terms, assuming a 100 % yield of CO from methane oxidation; this is only for diagnostic purposes and we do not make such assumptions in the actual mechanisms. Dry deposition of CO is a small loss term, particularly for the SH. TM5 and NIWA-UKCA

have comparable dry deposition loss rates. Note that CO loss through dry deposition is not included in GEOS-Chem and is not provided for CAM-chem.

The seasonal variation of CP and CL of CO in the SH are shown in Fig. 16. The surface emission of CO peaks in September in the SH which is dominated by biomass burning emissions. CPs and CLs maximise in austral summer and minimise in austral winter. CAM-chem shows much lower total CP and NMVOC oxidation compared to the other three models, in particular during the summer months, indicating below-average oxidizing capacity in that model. Examining the contribution to the total CPs, methane oxidation and oxidation from NMVOCs are nearly equal in all models except CAM-chem where NMVOC oxidation is significantly lower than methane oxidation. Methane oxidation is largest in GEOS-chem, followed by NIWA-UKCA reflecting the higher OH in these two models. The peak chemical loss shown in all four models in October is in response to the peak of surface emissions of CO. We also display the ratio of CO production from NMVOCs to the total CP, showing that TM5 has the highest ratio, indicating a fast conversion of NMVOCs to CO in TM5. In comparison, CAM-chem has a substantially lower NMVOC oxidation to total CP ratio, indicating a slower NMVOC to CO conversion; this is the primary cause for low CO in this model. We have not
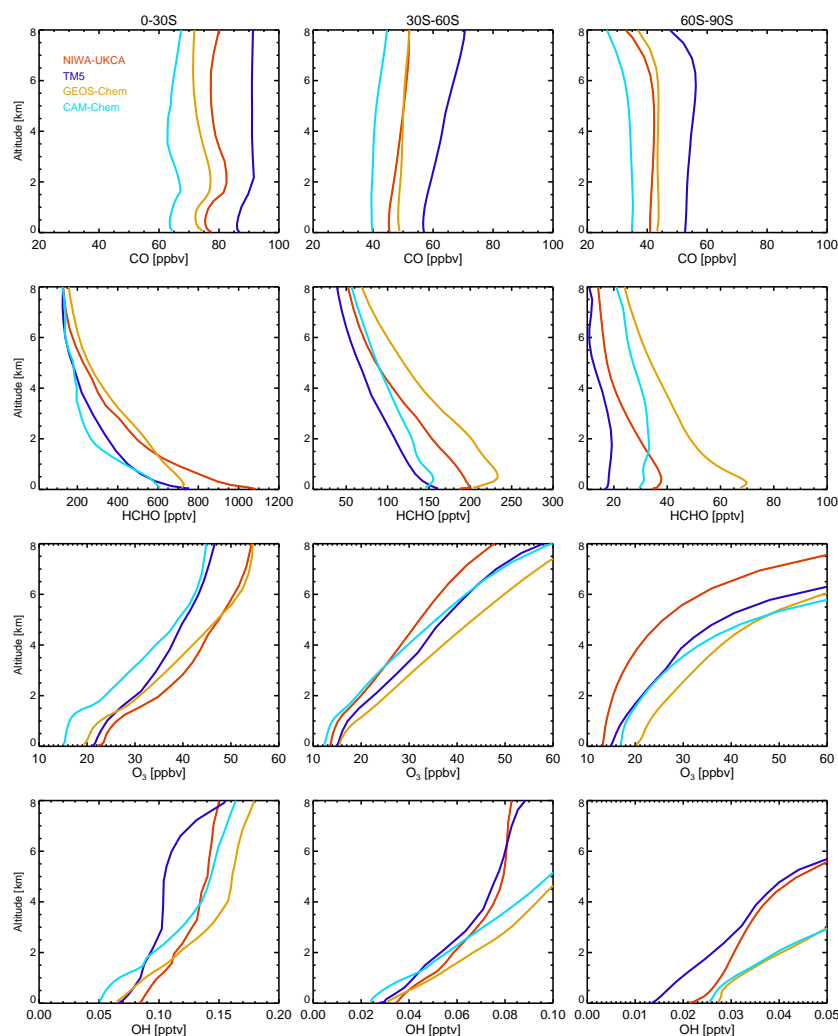
Figure 15. Monthly mean mixing ratios averaged over three SH regions (0–30, 30–60, and 60–90° S) for CO, HCHO, O$_3$, and OH. Data are for January 2005.

explicitly quantified the CO production from isoprene oxidation but assume that isoprene oxidation is the dominant contributor to NMVOC oxidation in the SH (Pfister et al., 2008). We therefore suggest that the different isoprene oxidation schemes used in the models are responsible for the differences in the chemical production rates of CO. Without a detailed comparison of the chemical mechanisms used in the models, we cannot identify which processes and/or parameters that make up the mechanisms are responsible for the differences in the models employed here, and such tests would be more suitably done in a box model in which parameters can be more straightforwardly controlled (e.g. Archibald et al., 2010). Four different isoprene oxidation mechanisms are included in the models presented here. They vary in complexity and also in the approaches to treat degradation products. The isoprene oxidation mechanism in NIWA-UKCA is based on a smaller mechanism (Mainz Isoprene Mechanism (MIM); Pöschl et al., 2000) than those used in GEOS-

Chem (Paulot et al., 2009a, b) and in CAM-chem (Emmons et al., 2010). NIWA-UKCA contains some recently updated rate coefficients of reactions between NO and peroxy radicals from the OH-initiated isoprene oxidation reactions, and reactions between OH and isoprene nitrate (Paulot et al., 2009a, b). The isoprene oxidation scheme in TM5 is based on the CB05 chemical mechanism (Yarwood et al., 2005) with modifications made to both the oxidation rates of peroxides and the production efficiency of HO$_2$ from the OH-initiated oxidation of isoprene based on recommendations by Archibald et al. (2010). Our results here show that the rates of NMVOC oxidation are substantially faster in TM5 (shown in Table 4 and Fig. 16) than in the other models, and such faster NMVOC oxidation rates are largely driven by the isoprene oxidation scheme in that model, which, together with the lower OH (shown in Table 6), lead to higher CO than in the other models.

Table 4. Tropospheric CO budget for 2004. Units in $\mathrm{TgCO\,yr^{-1}}$

	Global		SH		0–30° S		30–60° S		60–90° S	
	M	G	M	G	M	G	M	G	M	G
NIWA-UKCA										
Surface emission	1010	1010	306	306	288	288	18	18	0.3	0.3
Total CP	1887	1786	821	742	718	631	97	103	5.8	6.2
CH_4 oxidation*	1067	1086	437	451	353	367	78	76	5.0	5.2
NMVOC oxidation**	820	700	384	291	365	264	19	27	0.8	1.0
Chemical loss	2790	2668	1057	986	871	814	170	157	15	15
Dry deposition	101	98	27	25	25	23	2.0	1.6	0.0	0.0
TM5										
Surface emission	1010	1010	306	306	288	288	18	18	0.3	0.3
Total CP	1650	1535	743	663	654	565	86	94	3.9	4.2
CH_4 oxidation	865	927	361	390	284	312	73	74	3.7	3.9
NMVOC oxidation	785	618	382	273	370	253	13	20	0.2	0.3
Chemical loss	2516	2410	1016	941	801	748	201	180	14	13
Dry deposition	115	107	36	32	33	29	2.3	2.1	0.5	0.5
GEOS-Chem										
Surface emission	1010	1010	306	306	288	288	18	18	0.3	0.3
Total CP	1686	1670	770	729	646	600	116	121	8.0	8.2
CH_4 oxidation	1046	1072	455	470	360	375	89	90	5.6	5.7
NMVOC oxidation	640	598	315	259	286	225	27	31	2.4	2.5
Chemical loss	2749	2689	1142	1088	897	855	224	212	22	21
CAM-chem										
Surface emission	1010	1010	306	306	288	288	18	18	0.3	0.3
Total CP	1263	1210	552	504	465	415	82	84	4.8	4.9
CH_4 oxidation	862	890	364	383	282	301	77	77	4.7	4.8
NMVOC oxidation	401	320	188	121	183	114	5	7	0.1	0.1
Chemical loss	2068	2021	804	771	632	612	159	147	13	13

M: CLM-MEGANv2.1 emissions; G: LPJ-GUESS emissions; CP: chemical production; units in $\mathrm{Tg\,yr^{-1}}$;
* A conversion factor of 1.0 from methane oxidation is assumed here for diagnostic purposes;
** NMVOC oxidation is derived from total chemical production and methane oxidation, i.e. $CP_{\mathrm{NMVOCs}} = CP_{\mathrm{Total}} - CP_{\mathrm{CH_4}}$.

HCHO budget terms from NIWA-UKCA and TM5 are listed in Table 5 (These terms were not saved in the other models). The surface emissions of HCHO are small compared to the in situ chemical production and loss terms. The global total CP in NIWA-UKCA is slightly larger than in TM5 for both simulations, but the amounts are comparable for the SH. Methane oxidation rates are higher in NIWA-UKCA for all regions due to the higher OH in that model, and NMVOC oxidation rates are significantly larger in TM5. Examining the chemical losses, HCHO loss through the reaction with OH is much higher in NIWA-UKCA; however, HCHO losses through photolysis are comparable between these two models. Together with the smaller burden of HCHO in TM5, this implies that HCHO photolysis rates are larger in TM5 than in NIWA-UKCA. (This diagnostic is not directly available for either model.) The much larger wet deposition of HCHO in TM5 (i.e., ∼ 10 % of the to-

tal loss terms), compared to that in NIWA-UKCA (∼ 3 %), could explain the lower HCHO burden/columns in TM5. An additional hydration of HCHO is applied in TM5 (but not in the other models), which further enhances the effective solubility of HCHO in aqueous solution (Huijnen et al., 2010). This may have resulted in an additional loss of HCHO to wet deposition in TM5 which is however still substantially smaller than the gas-phase loss processes. The Henry's law coefficients, governing gas- and liquid-phase partitioning of HCHO, applied in the other models are comparable.

6 Sensitivity of modelled SH CO and HCHO to uncertainties in biogenic emissions

In Sect. 3, we showed the model deviations in CO and HCHO columns from observed FTIR values at four remote SH sites using two different biogenic emissions invento-

Table 5. Tropospheric HCHO budget for year 2004. Units in $Tg(HCHO) \, yr^{-1}$.

	Global		SH		0–30° S		30–60° S		60–90° S	
	M	G	M	G	M	G	M	G	M	G
				NIWA-UKCA						
Total source	1839	1764	777	723	672	612	101	105	6.2	6.6
Surface emission	13	13	4.9	4.9	4.7	4.7	0.2	0.2	0.0	0.0
Total CP	1826	1751	772	718	667	607	101	103	6.2	6.6
CP from CH_4	1137	1164	468	483	378	393	83	83	5.3	5.6
CP from NMVOC	689	587	304	235	289	214	17	20	0.9	1.0
Total sinks	1839	1764	780	726	672	612	102	107	6.3	6.7
OH + HCHO	507	519	190	193	170	172	20	20	0.5	0.5
HCHO + $h\nu$	1248	1170	553	502	471	415	76	81	5.5	6.0
Dry deposition	24	21	10	9	9	7	1.3	1.5	0.0	0.0
Wet deposition	58	53	26	23	22	18	4	4.4	0.1	0.4
				TM5						
Total source	1748	1647	777	704	674	593	99	106	4.1	4.4
Surface emission	13	13	4.9	4.9	4.7	4.7	0.2	0.2	0.0	0.0
Total CP*	1735	1634	772	699	670	588	99	106	4.1	4.4
CP from CH_4	927	993	387	418	304	334	79	80	2.2	2.3
CP from NMVOC	808	641	385	281	366	254	20	25	1.9	2.1
Total sinks	1748	1647	777	704	674	593	99	106	4.1	4.4
OH + HCHO	293	317	106	115	93	101	13	14	0.2	0.2
HCHO + $h\nu$	1247	1156	577	515	499	430	75	81	3.4	3.6
Dry deposition	34	28	13	10	12	9	1	1	0.0	0.0
Wet deposition	174	146	81	64	70	53	10	10	0.5	0.6

* Total chemical productions in TM5 are balanced by total sinks and surface emissions.

Table 6. Tropospheric CO, HCHO, and OH burden for year 2004.

	Global		SH		0–30° S		30–60° S		60–90° S	
	M	G	M	G	M	G	M	G	M	G
				NIWA-UKCA						
CO (Tg)	341	319	134	120	84	74	40	36	10	9.5
HCHO (Gg)	912	846	471	429	378	330	85	90	7	8
OH (Mg)	206	216	133	141	94	101	32	33	6.7	7.1
				TM5						
CO (Tg)	377	331	174	143	105	84	54	46	15	13
HCHO (Tg)	770	714	357	308	305	254	50	52	2.0	2.1
OH (Mg)	196	216	85	96	65	75	18	20	1.6	1.7
				GEOS-Chem						
CO (Tg)	323	307	142	130	86	77	46	42	12	11
HCHO (Gg)	1052	1045	473	451	372	346	90	93	11	11
OH (Mg)	262	272	120	126	91	96	26	27	2.9	3.0
				CAM-chem						
CO (Tg)	264	246	113	100	72	63	33	30	8.2	7.6
HCHO (Gg)	733	700	320	291	258	227	57	59	4.6	4.7
OH (Mg)	207	221	92	101	69	77	21	21	2.3	2.3

ries (for isoprene and monoterpenes), and found that modelled CO columns with LPJ-GUESS biogenic emissions are consistently lower and less representative of observed values than those produced using CLM-MEGANv2.1 emissions
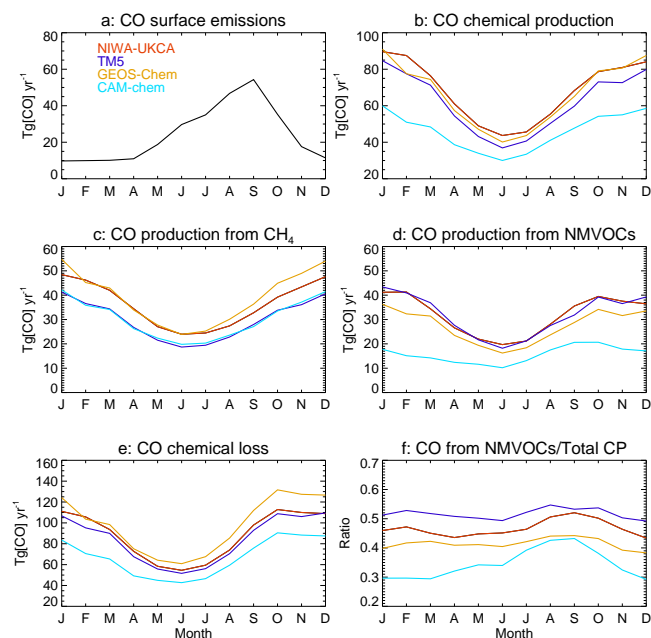
Figure 16. Monthly CO surface emissions, chemical production and loss terms, and the ratio of NMVOC oxidation to total chemical production in the SH. Data are for 2004.

(Table 3). Here we further quantify the changes in CO and HCHO columns in response to changes in biogenic emissions at the hemispheric scale, and also highlight associated changes in the corresponding OH columns. Figures 17–19 display the monthly mean global distributions of relative differences in CO, HCHO, and OH columns between simulations using CLM-MEGANv2.1 and LPJ-GUESS, respectively, for January and July (averaged over 2004–2008). The differences calculated for all species are expressed as the percentage change relative to the CLM-MEGANv2.1 simulation. Here, we show results for the January and July months in order to contrast the seasonal features in oxidizing capacity. For all models, applying LPJ-GUESS emissions results in significant decreases in CO columns throughout the SH, with the largest decreases in the South American and Australian source regions (Fig. 17), in response to the smaller emission fluxes of isoprene and monoterpenes from LPJ-GUESS (the accumulated peak isoprene emissions in CLM-MEGANv2.1 are 25 % higher than in LPJ-GUESS during the peak season of the austral summer months, shown in Fig. 1, and the biggest differences are in South America). Away from these source regions, the differences are largely homogeneous in the mid- to high latitudes. The models' responses to changes in biogenic emissions vary considerably, with TM5 having the largest sensitivity of CO columns change to changes in biogenic emissions, namely ∼ 35 % in January and ∼ 25 % in July in the source regions and 10–15 % over the remote SH. GEOS-Chem has the lowest sensitivity with 15–20 % changes in January and 10–15 % in July in the source regions

and less than 10 % in remote regions in response to the same emission changes of isoprene and monoterpenes.

For corresponding changes in tropospheric HCHO columns (Fig. 18), substantial decreases (up to ∼ 50–60 %) occur in the source regions of South America and Australia in response to smaller emission fluxes in LPJ-GUESS, relative to CLM-MEGANv2.1. These reductions in HCHO columns propagate to the sub-tropical remote oceans where the magnitude of the decreases is greatly reduced. There are some increases in HCHO columns over southern Africa, which are responses to the higher isoprene emissions in LPJ-GUESS. However, there is a consistent increase of up to 5 % over large areas of the mid- to high latitudes which is apparently not directly caused by reduced biogenic emissions. We find that changes in both CO and HCHO are associated with changes in OH (Fig. 19); the tropospheric OH columns exhibit substantial increases in the source regions as a result of reduced isoprene and monoterpene emissions; qualitatively these effects follow the differences in the geographical distributions of the emissions, and are of opposite sign to both the CO and the HCHO columns changes there. OH increases in remote regions are largely positive, and are opposite in sign to the CO changes; i.e. reduced loss rates of CO cause increases in OH. However, increases in OH columns away from the source regions correlate with HCHO changes; this implies that increases in HCHO in remote regions under LPJ-GUESS emissions are due to strengthened methane oxidation through increases in OH. The inter-model differences in HCHO changes are generally small in remote regions; TM5 shows the largest sensitivity over the source regions in both OH and HCHO, due primarily to the faster isoprene oxidation processes in that model. Note that the large relative differences in both HCHO and OH in July at high latitudes shown in CAM-chem are not significant because the background abundances of both species in the polar region are extremely small.

In Table 7 we summarise hemispheric changes in chemical production and loss rates of tropospheric CO and HCHO, in response to the differences in biogenic emissions. Values expressed are percentage changes (i.e. LPJ-GUESS minus CLM-MEGANv2.1 relative to CLM-MEGANv2.1), and are given for both hemispheres to assess the hemispheric impact of biogenic emissions. In the SH, the changes in all terms are negative, except for the rates of chemical production of both CO and HCHO from methane oxidation; this is generally the result of increased OH in the LPJ-GUESS simulation, in response to reduced biogenic emissions in that inventory. For all models, relative reductions in NMVOC oxidation rates (−17.8 to −35.6 %) are substantially larger than relative increases in CP from methane oxidation (3.2 to 8.0 %), in response to changes in biogenic emissions. Therefore, NMVOC oxidation (mainly of isoprene) is the driving factor for model differences in in situ CO and HCHO production. The burden changes are closely related to the changes in total CP; i.e. TM5 has the largest changes in both bur-
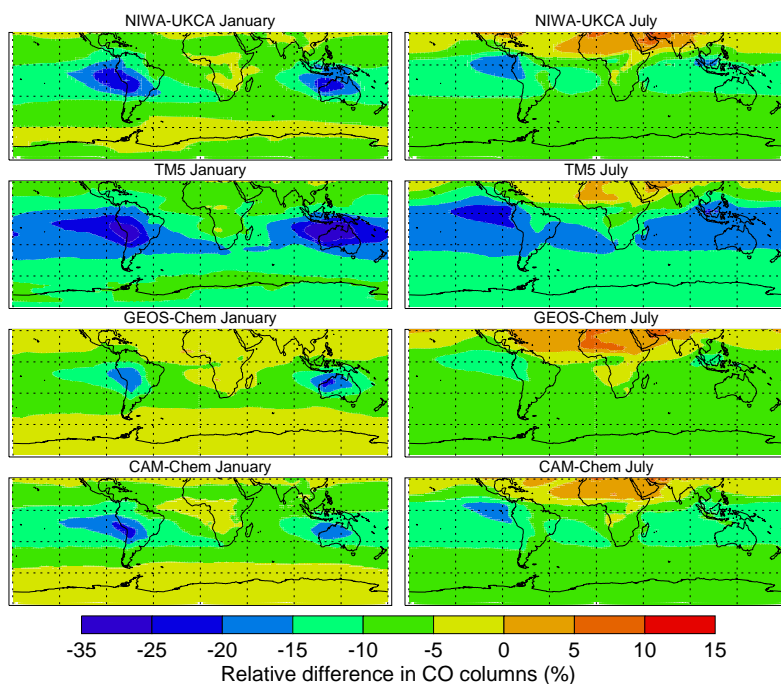
Figure 17. Relative differences (%) in modelled CO columns between the LPJ-GUESS and the CLM-MEGANv2.1 simulations from four models for January (left) and July (right). Results are expressed as "$100 \times (CO_{LPJ\text{-}GUESS} - CO_{CLM\text{-}MEGANv2.1})/CO_{CLM\text{-}MEGANv2.1}$". Data are averaged over 2004–2008.
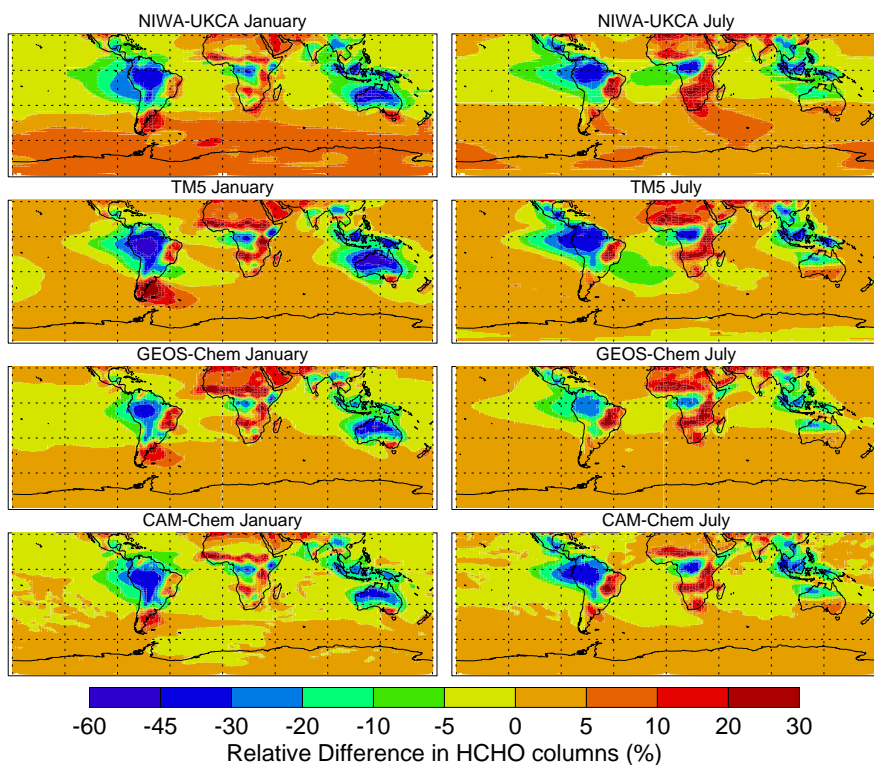

Figure 18. Same as Fig. 17, but for HCHO.

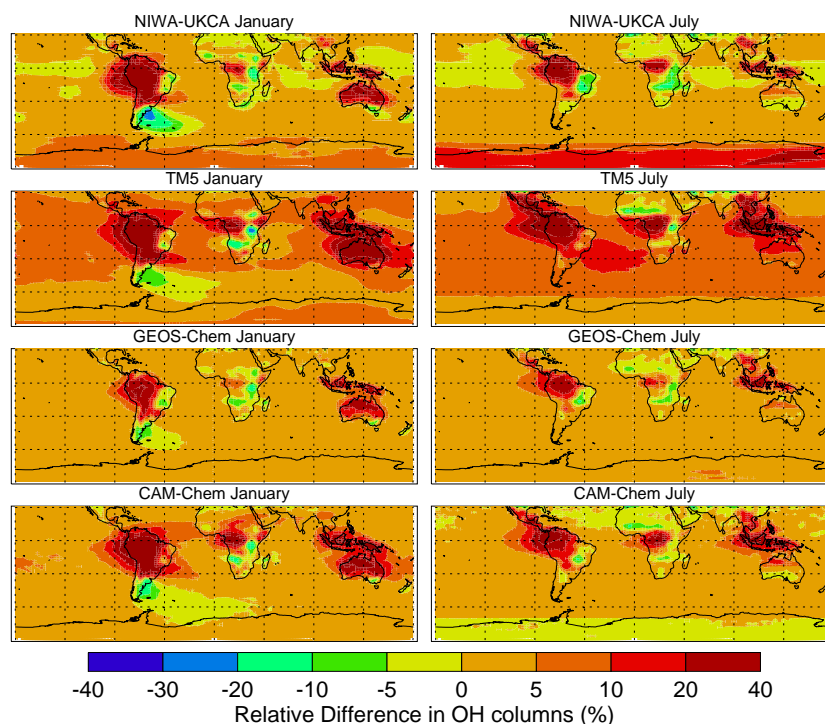**Figure 19.** Same as Fig. 17, but for OH.

Table 7. Relative differences (%) in tropospheric CO budget terms between CLM-MEGANv2.1 and LPJ-GUESS simulations for 2004.

| | Total CP | | CP CH$_4$ | | CP NMVOCs | | Total CL | | Burden | |
	NH	SH	NH	SH	NH	SH	NH	SH	NH	SH
					CO					
NIWA-UKCA	−2.1	−9.6	0.8	3.2	−6.2	−24.2	−2.9	−6.7	−3.9	−10.4
TM5	−3.9	−10.7	6.5	8.0	−14.4	−28.5	−2.1	−7.4	−7.4	−17.8
GEOS-Chem	2.7	−5.3	1.9	3.3	4.3	−17.8	−0.4	−4.7	−2.2	−8.5
CAM-chem	−0.7	−8.7	1.8	5.2	−6.6	−35.6	−1.1	−4.1	−3.3	−11.5
					HCHO					
NIWA-UKCA	−2.0	−7.0	1.8	3.2	−8.6	−22.7	−1.8	−6.5	−5.4	−8.9
TM5	−2.9	−9.5	6.5	8.0	−14.9	−27.5	−1.6	−7.8	−1.7	−13.7

Differences calculated as $100\times$(LPJ-GUESS − CLM-MEGANv2.1)/CLM-MEGANv2.1.

den and the CP, and GEOS-Chem has the smallest terms for both. For all models, relative responses in the SH are much larger than in the NH, emphasizing the importance of biogenic emissions for CO and HCHO formation in the SH.

Complementing the comparison of columns, we here compare the seasonal differences in vertical profiles of CO mixing ratios between CLM-MEGANv2.1 and LPJ-GUESS simulations, averaged zonally and over 2004 to 2008. Figure S5 in the Supplement shows large reductions in CO over the SH tropics in all simulations using LPJ-GUESS emissions of isoprene and monoterpenes, relative to those using CLM-MEGANv2.1, and these reductions propagate to the upper

SH tropical troposphere and spread throughout the middle and high latitudes. This shows that the CO column changes in the extratropics are dominated by the changes in the free and upper troposphere, where CO has a relatively long lifetime. Overall, the impact of biogenic emissions on CO are more significant in the SH than the NH. In the SH, throughout the depth of the troposphere, the LPJ-GUESS simulations have reduced CO, which is linked to much reduced CO in the tropics. This effect maximizes during austral winter and spring.

7 Summary and conclusions

We have compared modelled daily-mean CO and HCHO columns from a four-model ensemble with the observed daily-mean FTIR columns of these two species at SH sites including the tropical site Darwin, the mid-latitude sites Wollongong and Lauder, and the Antarctic site Arrival Heights for CO, and Wollongong and Lauder for HCHO. We use CLM-MEGANv2.1 biogenic emissions for the first set of simulations; for these simulations modelled and measured CO are in reasonable agreement, albeit with some low biases, in all models at most locations; annually averaged deviations relative to the observations are -3.2% at Arrival Heights, -8.6% at Lauder, -19.2% at Wollongong, and -6.9% at Darwin for the four-model mean. The largest discrepancies between modelled and observed CO columns occur at Wollongong which is heavily influenced by local urban and industrial sources and episodic nearby bush fires that are most likely unaccounted for in the emission inventories. Large inter-model differences exist at all locations for all seasons with the exception of austral spring at Darwin where the local biomass burning sources dominate the CO columns. We also compare the modelled surface CO to observations; significant inter-model differences exist although the ensemble mean exhibits good agreement with the observed values for most sites. The inter-model differences for modelled surface CO are markedly larger than the differences between the ensemble mean and observed surface CO. In agreement with previous modelling studies of HCHO in the remote SH (Ayers et al., 1997; Jones et al., 2009; Vigouroux et al., 2009), the models significantly underestimate observed HCHO columns at Wollongong and Lauder by more than a factor of 2, and the largest discrepancy occurs during austral summer. We cannot reconcile such significant differences between the modelled and observed HCHO columns over the remote SH with our current understanding. We hypothesize that missing local sources and/or missing chemical processes are the most likely causes. The fact that model differences are much smaller than the differences between the models and the observations indicate that the cause of such a large discrepancy probably goes beyond what the differences in chemical mechanisms can explain.

To determine the sensitivity of CO and HCHO distributions to biogenic emissions, we perform a second set of simulations with emissions of isoprene and monoterpenes from the LPJ-GUESS data set; results show that the LPJ-GUESS simulations exhibit systematically lower CO columns and lower surface CO than the CLM-MEGANv2.1 simulations, in response to an average of $\sim$9 % reduction in isoprene emissions globally and a $\sim$17 % reduction in the SH (monoterpene emissions are also substantially lower in LPJ-GUESS; see Table 1). Annually averaged relative differences between ensemble model mean and observed CO columns are -10.5% at Arrival Heights, -17.1% at Lauder, -27.5% at Wollongong, and -19.9% at Darwin. The differences in surface CO at remote monitoring sites between the two simulations are generally smaller than 5 %. At neither Wollongong nor Lauder do we find that differences in biogenic emissions have any significant impact on modelled HCHO columns.

Examining the response of CO and HCHO columns to differences in biogenic emissions of isoprene and monoterpenes on the hemispheric scale, we show that both species exhibit large sensitivity to emissions in the source regions, with 30–40 % reductions in CO and HCHO columns, as a direct consequence of the mainly reduced emissions of isoprene and monoterpenes in the LPJ-GUESS inventory, relative to CLM-MEGANv2.1 (i.e. $\sim$ 37 % reduction of isoprene emissions in Australia and Indonesia, $\sim$ 23 % reduction in South America, and $\sim$ 13 % overall increase in Africa, with both increases and reductions occurring in different regions), and these reductions in CO and HCHO are generally larger in summer than in winter. Away from the source regions and throughout the SH, decreases in CO columns are roughly half those occurring in the source regions, whereas there are moderate increases in HCHO columns ($\sim$ 5 %) despite the significant decreases in and near the source regions for all models. We show that the increases in HCHO columns in the remote SH for LPJ-GUESS, relative to CLM-MEGANv2.1, are linked to the increases in OH columns through enhanced methane oxidation in the remote SH (see Tables 5 and 6). There are substantial increases in OH columns in the source regions in direct response to the reduced isoprene and monoterpene emissions in the LPJ-GUESS inventory, whereas the general increase (up to $\sim$ 5 % across the models) in the remote regions is the result of reductions in CO and possibly other longer-lived isoprene oxidation products.

Significant inter-model differences exist in modelled CO columns; we quantify these differences in three latitudinal regions (SH tropics, mid-, and high latitudes). The ratios of individual model columns to the ensemble-mean columns (annually averaged and averaged across the three regions) are between 0.85 and 1.15 for the tropical region, and the range increases to between 0.7 and 1.2 at high latitudes. Using diagnostic tracers, we assess the impact of modelled transport (by CO_{25}), the contribution from primarily emitted CO (by CO_{OH}), and CO produced and transported from secondary CO production ($CO_{sec} = CO - CO_{OH}$). The results reveal that the differences in transport are not sufficient to explain the differences in modelled CO columns. The modelled range of CO_{OH} corresponds much better to the modelled CO columns than CO_{25} but still cannot fully explain the inter-model differences in modelled CO columns. The differences in secondary CO production, i.e. CO_{sec}, however, correspond well with those in modelled CO columns. TM5 exhibits the highest values in both variables, followed by GEOS-Chem, NIWA-UKCA, and CAM-chem in magnitude. We calculate that CO_{sec} contributes around 65 % to CO in the tropics and around 75 % in the polar region in each model, and is responsible for two-thirds of the inter-model differences in mod-

elled CO columns overall. This suggests that the models' differences in secondary CO production from methane and NMVOC oxidation play a major role in their ability to reproduce the CO columns in the SH, as also noted by Fisher et al. (2015).

We further quantify the models' differences in chemistry by examining the chemical production and loss terms of CO and HCHO in the models. Results show that large differences in chemical production between the models are largely attributed to differences in the rates of NMVOC oxidation, which are mainly driven by the differences in isoprene oxidation processes, which exhibit varying degrees of complexity in the models. We show the collective effects that different isoprene oxidation schemes have on the rates of chemical production of CO and HCHO but are not able to individually quantify which reactions/processes are responsible for the differences in modelled CO and HCHO. Among the four models, NIWA-UKCA has the highest total chemical production rates of CO, followed by GEOS-Chem, TM5, and CAM-chem which has the lowest chemical production rates. Methane oxidation rates are mainly driven by the OH abundance in the models with TM5 having the lowest OH hence the lowest methane oxidation rates. The fastest conversion rates from NMVOCs to CO occurs in TM5, and the slowest in CAM-chem, leading to respectively high and low CO in these two models. Modelled CO in NIWA-UKCA and GEOS-Chem both better matches the observations in general, irrespective of the different complexities of the isoprene oxidation schemes employed in these two models. Moreover, GEOS-Chem includes some recent advances in isoprene oxidation mechanisms, for example, OH formation of epoxide species which regenerate OH under low NO_x conditions (Paulot et al., 2009b). Epoxides are not included in other models. We have not specifically tested how recent experimental evidence on isoprene oxidation mechanisms, e.g. OH regeneration in a low-NO_x environment (Fuchs et al., 2013), will impact on modelled species. More detailed and targeted studies will be needed to clarify how individual approaches/processes making up isoprene oxidation schemes will impact chemical production of CO and HCHO in global models.

Production and loss terms of HCHO are assessed in NIWA-UKCA and TM5. We find that total chemical productions are comparable in the two models, with moderately larger chemical production and loss rates in NIWA-UKCA. Again, the production of HCHO from the oxidation of NMVOCs is faster in TM5 although this is partly offset, for HCHO production, by the slower methane oxidation rates due to lower OH. The markedly lower HCHO in TM5 than in NIWA-UKCA could be due to the substantially larger wet deposition loss rate of HCHO, and a faster photodissociation rate of HCHO in TM5. Despite the differences in rates of HCHO formation and loss, we cannot, based on these differences alone, explain the substantial low bias in modelled HCHO in all models compared to the observed HCHO

columns at Lauder and Wollongong. We therefore suspect that missing local sources and/or HCHO precursors might contribute to the differences between modelled and observed HCHO.

We conclude that the uncertainty in biogenic emissions remains a significant problem in modelling both long- and short-lived species throughout the SH. Understanding the differences between isoprene oxidation mechanisms and the resultant differences in modelled CO and HCHO is critical, and might result in an improvement in these mechanisms, allowing for a more robust use of HCHO and CO columns to constrain biogenic emissions and reduce this uncertainty. Given that the differences between the two biogenic emissions inventories used here are moderate compared to the much larger uncertainties existing in the current estimates of isoprene and monoterpene emissions, the resultant uncertainty in modelled CO could be much larger. Although the ensemble model mean satisfactorily compares to observed CO in the SH, the large inter-model differences add more uncertainties in modelled CO and in constraining biogenic emissions. Note that in this paper, we do not separately quantify the effect from changes in monoterpene emissions. The emissions from monoterpenes are around 30 and 10 % of those of isoprenes in CLM-MEGANv2.1 and LPJ-GUESS inventories, respectively, which could have a significant impact on modelled CO. However, due to the large uncertainty in emissions and the varying degrees of complexity of the monoterpene degradation schemes included in each model, this will further complicate the interpretation of the impact from changing monoterpene emissions.

The Supplement related to this article is available online at doi:10.5194/acp-15-7217-2015-supplement.

Edited by: A. Pozzer

References

Archibald, A., Jenkin, M., and Shallcross, D.: An isoprene mechanism intercomparison, Atmos. Environ., 44, 5356–5364, 2010.

Arneth, A., Miller, P. A., Scholze, M., Hickler, T., Schurgers, G., Smith, B., and Prentice, I. C.: CO$_2$ inhibition of global terrestrial isoprene emissions: potential implications for atmospheric chemistry, Geophys. Res. Lett., 34, L18813, doi:10.1029/2007GL030615, 2007a.

Arneth, A., Niinemets, Ü., Pressley, S., Bäck, J., Hari, P., Karl, T., Noe, S., Prentice, I. C., Serça, D., Hickler, T., Wolf, A., and Smith, B.: Process-based estimates of terrestrial ecosystem isoprene emissions: incorporating the effects of a direct CO$_2$-isoprene interaction, Atmos. Chem. Phys., 7, 31–53, doi:10.5194/acp-7-31-2007, 2007b.

Arneth, A., Monson, R. K., Schurgers, G., Niinemets, Ü., and Palmer, P. I.: Why are estimates of global terrestrial isoprene emissions so similar (and why is this not so for monoterpenes)?, Atmos. Chem. Phys., 8, 4605–4620, doi:10.5194/acp-8-4605-2008, 2008.

Atkinson, R.: Atmospheric chemistry of VOCs and NO$_x$, Atmos. Environ., 34, 2063–2101, 2000.

Atkinson, R., Baulch, D. L., Cox, R. A., Crowley, J. N., Hampson, R. F., Hynes, R. G., Jenkin, M. E., Rossi, M. J., Troe, J., and IUPAC Subcommittee: Evaluated kinetic and photochemical data for atmospheric chemistry: Volume II – gas phase reactions of organic species, Atmos. Chem. Phys., 6, 3625–4055, doi:10.5194/acp-6-3625-2006, 2006.

Ayers, G. P., Gillett, R. W., Granek, H., de Serves, C., and Cox, R. A.: Formaldehyde production in clean marine air, Geophys. Res. Lett., 24, 401–404, 1997.

Barkley, M. P., Palmer, P. I., Kuhn, U., Kesselmeier, J., Chance, K., Kurosu, T. P., Martin, R. V., Helmig, D., and Guenther, A.: Net ecosystem fluxes of isoprene over tropical South America inferred from Global Ozone Monitoring Experiment (GOME) observations of HCHO columns, J. Geophys. Res., 113, D20304, doi:10.1029/2008JD009863, 2008.

Bey, I., Jacob, D. J., Yantosca, R. M., Logan, J. A., Field, B. D., Fiore, A. M., Li, Q. B., Liu, H. Y., Mickley, L. J., and Schultz, M. G.: Global modeling of tropospheric chemistry with assimilated meteorology: model description and evaluation, J. Geophys. Res., 106, 23073–23095, 2001.

Bonsang, B., Polle, C., and Lambert, G.: Evidence for marine production of isoprene, Geophys. Res. Lett., 19, 1129–1132, 1992.

Brasseur, G. P., Hauglustaine, D. A., Walters, S., and Rasch, P. J.: MOZART, a global chemical transport model for ozone and related chemical tracers, 1, Model description, J. Geophys. Res., 103, 28265–28289, 1998.

DeCaria, A. J., Pickering, K. E., Stenchikov, G. L., and Ott, L. E.: Lightning-generated NO$_x$ and its impact on tropospheric ozone production: a three-dimensional modeling study of a Stratosphere–Troposphere Experiment: Radiation, Aerosols and Ozone (STERAO-A) thunderstorm, J. Geophys. Res., 110, D14303, doi:10.1029/2004JD005556, 2006.

Dee, D. P., Uppala, S. M., Simmons, A. J., Berrisford, P., Poli, P., Kobayashi, S., Andrae, U., Balmaseda, M. A., Balsamo, G., Bauer, P., Bechtold, P., Beljaars, A. C. M., van de Berg, L., Bidlot, J., Bormann, N., Delsol, C., Dragani, R., Fuentes, M., Geer, A. J., Haimberger, L., Healy, S. B., Hersbach, H., Hólm, E. V., Isaksen, L., Kållberg, P., Köhler, M., Matricardi, M., McNally, A. P., Monge-Sanz, B. M., Morcrette, J.-J., Park, B.-K., Peubey, C., de Rosnay, P., Tavolato, C., Thépaut, J.-N., and Vitart, F.: The ERA-Interim reanalysis: configuration and performance of the data assimilation system, Q. J. Roy. Meteor. Soc., 137, 553–597, 2011.

Deeter, M. N., Emmons, L. K., Francis, G. L., Edwards, D. P., Gille, J. C., Warner, J. X., Khattatov, B., Ziskin, D., Lamarque, J.-F., Ho, S.-P., Yudin, V., Attié, J.-L., Packman, D., Chen,J., Mao, D., and Drummond, J. R.: Operational carbon monoxide retrieval algorithm and selected results for the MOPITT instrument, J. Geophys. Res., 108, 4399, doi:10.1029/2002JD003186, 2003.

Deeter, M. N., Martínez-Alonso, S., Edwards, D. P., Emmons, L. K., Gille, J. C., Worden, H. M., Sweeney, C., Pittman, J. V., Daube, B. C., and Wofsy, S. C.: The MOPITT Version 6 product: algorithm enhancements and validation, Atmos. Meas. Tech., 7, 3623–3632, doi:10.5194/amt-7-3623-2014, 2014.

de Laat, A. T. J., Gloudemans, A. M. S., Schrijver, H., Aben, I., Nagahama, Y., Suzuki, K., Mahieu, E., Jones, N. B., Paton-Walsh, C., Deutscher, N. M., Griffith, D. W. T., De Mazière, M., Mittermeier, R. L., Fast, H., Notholt, J., Palm, M., Hawat, T., Blumenstock, T., Hase, F., Schneider, M., Rinsland, C., Dzhola, A. V., Grechko, E. I., Poberovskii, A. M., Makarova, M. V., Mellqvist, J., Strandberg, A., Sussmann, R., Borsdorff, T., and Rettinger, M.: Validation of five years (2003–2007) of SCIAMACHY CO total column measurements using ground-based spectrometer observations, Atmos. Meas. Tech., 3, 1457–1471, doi:10.5194/amt-3-1457-2010, 2010.

Deutscher, N. M., Griffith, D. W. T., Bryant, G. W., Wennberg, P. O., Toon, G. C., Washenfelder, R. A., Keppel-Aleks, G., Wunch, D., Yavin, Y., Allen, N. T., Blavier, J.-F., Jiménez, R., Daube, B. C., Bright, A. V., Matross, D. M., Wofsy, S. C., and Park, S.: Total column CO$_2$ measurements at Darwin, Australia – site description and calibration against in situ aircraft profiles, Atmos. Meas. Tech., 3, 947–958, doi:10.5194/amt-3-947-2010, 2010.

Duncan, B. N., Logan, J. A., Bey, I., Megretskaia, I. A., Yantosca, R. M., Novelli, P. C., Jones, N. B., and Rinsland, C. P.: Global budget of CO, 1988–1997: source estimates and validation with a global model, J. Geophys. Res., 112, D22301, doi:10.1029/2007JD008459, 2007.

Edwards, D. P., Emmons, L. K., Gille, J. C., Chu, A., Attié, J.-L., Giglio, L., Wood, S. W., Haywood, J., Deeter, M. N., Massie, S. T., Ziskin, D. C., and Drummond, J. R.: Satellite-observed pollution from Southern Hemisphere biomass burning, J. Geophys. Res., 111, D14312, doi:10.1029/2005JD006655, 2006.

Emmons, L. K., Walters, S., Hess, P. G., Lamarque, J.-F., Pfister, G. G., Fillmore, D., Granier, C., Guenther, A., Kinnison, D., Laepple, T., Orlando, J., Tie, X., Tyndall, G., Wiedinmyer, C., Baughcum, S. L., and Kloster, S.: Description and evaluation of the Model for Ozone and Related chemical Tracers, version 4 (MOZART-4), Geosci. Model Dev., 3, 43–67, doi:10.5194/gmd-3-43-2010, 2010.

Eyring, V., Lamarque, J.-F., Hess, P., Arfeuille, F., Bowman, K., Chipperfield, M. P., Duncan, B., Fiore, A., Gettelman, A., Giorgetta, M. A., Granier, C., Hegglin, M., Kinnison, D., Kunze, M., Langematz, U., Luo, B., Martin, R., Matthes, K., Newman, P. A., Peter, T., Robock, A., Ryerson, T., Saiz-Lopez, A., Salawitch, R., Schultz, M., Shepherd, T. G., Shindell, D., Stähelin, J., Tegtmeier, S., Thomason, L., Tilmes, S., Vernier, J.-P., Waugh, D. W.,

and Young, P. J.: Overview of IGAC/SPARC Chemistry–Climate Model Initiative (CCMI) community simulations in support of upcoming ozone and climate assessments, SPARC Newsletter, 40, 48–66, 2013.

Fisher, J. A., Jacob, D. J., Purdy, M. T., Kopacz, M., Le Sager, P., Carouge, C., Holmes, C. D., Yantosca, R. M., Batchelor, R. L., Strong, K., Diskin, G. S., Fuelberg, H. E., Holloway, J. S., Hyer, E. J., McMillan, W. W., Warner, J., Streets, D. G., Zhang, Q., Wang, Y., and Wu, S.: Source attribution and interannual variability of Arctic pollution in spring constrained by aircraft (ARCTAS, ARCPAC) and satellite (AIRS) observations of carbon monoxide, Atmos. Chem. Phys., 10, 977–996, doi:10.5194/acp-10-977-2010, 2010.

Fisher, J. A., Wilson, S. R., Zeng, G., Williams, J. E., Emmons, L. K., Langenfelds, R. L., Krummel, P. B., and Steele, L. P.: Seasonal changes in the tropospheric carbon monoxide profile over the remote Southern Hemisphere evaluated using multi-model simulations and aircraft observations, Atmos. Chem. Phys., 15, 3217–3239, doi:10.5194/acp-15-3217-2015, 2015.

Fishman, J., Fakhruzzaman, K., Cros, B., and Nganga, D.: Identification of widespread pollution in the Southern Hemisphere deduced from satellite analyses, Science, 252, 1693–1696, 1991.

Fuchs, H., Hofzumahaus, A., Rohrer, F., Bohn, B., Brauers, T., Dorn, H-P., Häseler, R., Holland, F., Kaminski, M., Li, X., Lu, K., Nehr, S., Tillmann, R., Wegener R., and Wahner, A.: Experimental evidence for efficient hydroxyl radical regeneration in isoprene oxidation, Nature Geosci., 6, 995–996, doi:10.1038/ngeo2022, 2013.

Gloudemans, A. M. S., Krol, M. C., Meirink, J. F., de Laat, A. T. J., van der Werf, G. R., Schrijver, H., van den Broek, M. M. P., and Aben, I.: Evidence for long-range transport of carbon monoxide in the Southern Hemisphere from SCIAMACHY observations, Geophys. Res. Lett., 33, L16807, doi:10.1029/2006GL026804, 2006.

Granier, C., Bessagnet, B., Bond, T., D'Angiola, A., Denier van der Gon, H., Frost, G. J., Heil, A., Kaiser, J. W., Kinne, S., Klimont, Z., Kloster, S.-F., Lamarque, J., Liousse, C., Masui, T., Meleux, F., Mieville, A., Ohara, T., Raut, J.-C., Riahi, K., Schultz, M. G., Smith, S. J., Thompson, A., van Aardenne, J., van der Werf, G. R., and van Vuuren, D. P.: Evolution of anthropogenic and biomass burning emissions of air pollutants at global and regional scales during the 1980–2010 period, Clim. Change, 109, 163–190, doi:10.1007/s10584-011-0154-1, 2011.

Guenther, A. B., Jiang, X., Heald, C. L., Sakulyanontvittaya, T., Duhl, T., Emmons, L. K., and Wang, X.: The Model of Emissions of Gases and Aerosols from Nature version 2.1 (MEGAN2.1): an extended and updated framework for modeling biogenic emissions, Geosci. Model Dev., 5, 1471–1492, doi:10.5194/gmd-5-1471-2012, 2012.

Hatakeyama, S., Izumi, K., Fukuyama, T., Akimoto, H., and Washida, N.: Reactions of OH with α-pinene and β-pinene in air: Estimate of global CO production from the atmospheric oxidation of terpenes, J. Geophys. Res., 96, 947–958, doi:10.1029/90JD02341, 1991.

Heald, C. L., Jacob, D. J., Fiore, A. M., Emmons, L. K., Gille, J. C., Deeter, M. N., Warner, J., Edwards, D. P., Crawford, J. H., Hamlin, A. J., Sachse, G. W., Browell, E. V., Avery, M. A., Vay, S. A., Westberg, D. J., Blake, D. R., Singh, H. B., Sandholm, S. T., Talbot, R. W., and Fuelberg, H. E.: Asian outflow and transpacific transport of carbon monoxide and ozone pollution: an integrated satellite, aircraft and model perspective, J. Geophys. Res., 108, 4804, doi:10.1029/2003JD003507, 2003.

Hewitt, H. T., Copsey, D., Culverwell, I. D., Harris, C. M., Hill, R. S. R., Keen, A. B., McLaren, A. J., and Hunke, E. C.: Design and implementation of the infrastructure of HadGEM3: the next-generation Met Office climate modelling system, Geosci. Model Dev., 4, 223–253, doi:10.5194/gmd-4-223-2011, 2011.

Holloway, T., Levy II, H., and Kasibhatla, P.: Global distribution of carbon monoxide, J. Geophys. Res., 105, 12123–12147, doi:10.1029/1999JD901173, 2000.

Huijnen, V., Williams, J., van Weele, M., van Noije, T., Krol, M., Dentener, F., Segers, A., Houweling, S., Peters, W., de Laat, J., Boersma, F., Bergamaschi, P., van Velthoven, P., Le Sager, P., Eskes, H., Alkemade, F., Scheele, R., Nédélec, P., and Pätz, H.-W.: The global chemistry transport model TM5: description and evaluation of the tropospheric chemistry version 3.0, Geosci. Model Dev., 3, 445–473, doi:10.5194/gmd-3-445-2010, 2010.

Jacob, D. J., Field, B. D., Jin, E. M., Bey, I., Li, Q., Logan, J. A., Yantosca, R. M., and Singh. H. B.: Atmospheric budget of acetone, J. Geophys. Res., 107, ACH 5-1–ACH 5-17, doi:10.1029/2001JD000694, 2002.

Jones, N. B., Rinsland, C. P., Liley, J. B., and Rosen, J.: Correlation of aerosol and carbon monoxide at 45° S: evidence of biomass burning emissions, Geophys. Res. Lett., 28, 709–712, 2001.

Jones, N. B., Riedel, K., Allan, W., Wood, S., Palmer, P. I., Chance, K., and Notholt, J.: Long-term tropospheric formaldehyde concentrations deduced from ground-based fourier transform solar infrared measurements, Atmos. Chem. Phys., 9, 7131–7142, doi:10.5194/acp-9-7131-2009, 2009.

Kurokawa, J., Ohara, T., Morikawa, T., Hanayama, S., Janssens-Maenhout, G., Fukui, T., Kawashima, K., and Akimoto, H.: Emissions of air pollutants and greenhouse gases over Asian regions during 2000–2008: Regional Emission inventory in ASia (REAS) version 2, Atmos. Chem. Phys., 13, 11019–11058, doi:10.5194/acp-13-11019-2013, 2013.

Lamarque, J.-F., Bond, T. C., Eyring, V., Granier, C., Heil, A., Klimont, Z., Lee, D., Liousse, C., Mieville, A., Owen, B., Schultz, M. G., Shindell, D., Smith, S. J., Stehfest, E., Van Aardenne, J., Cooper, O. R., Kainuma, M., Mahowald, N., McConnell, J. R., Naik, V., Riahi, K., and van Vuuren, D. P.: Historical (1850–2000) gridded anthropogenic and biomass burning emissions of reactive gases and aerosols: methodology and application, Atmos. Chem. Phys., 10, 7017–7039, doi:10.5194/acp-10-7017-2010, 2010.

Lamarque, J.-F., Emmons, L. K., Hess, P. G., Kinnison, D. E., Tilmes, S., Vitt, F., Heald, C. L., Holland, E. A., Lauritzen, P. H., Neu, J., Orlando, J. J., Rasch, P. J., and Tyndall, G. K.: CAM-chem: description and evaluation of interactive atmospheric chemistry in the Community Earth System Model, Geosci. Model Dev., 5, 369–411, doi:10.5194/gmd-5-369-2012, 2012.

Langenfelds, R., Francey, R., Steele, L., Fraser, P., Coram, S., Hayes, M., Beardsmore, D., Lucarelli, M., and de Silva, F.: Improved vertical sampling of the trace gas composition of the troposphere above Cape Grim since 1991, in: Baseline Atmospheric Program (Australia) 15 1993, edited by: Francey, R., Dick, A., and Derek, N., Bureau of Meteorology and CSIRO Division of Atmospheric Research, Melbourne, Australia, 45–56, 1996.

Lawrence, D. M., Oleson, K. W., Flanner, M. G., Thorton, P. E., Swenson, S. C., Lawrence, P. J., Zeng, X., Yang, Z.-L., Levis, S., Skaguchi, K., Bonan, G. B., and Slater, A. G.: Parameterization improvements and functional and structural advances in version 4 of the Community Land Model, J. Adv. Model. Earth Sys., 3, M03001, doi:10.1029/2011ms000045, 2011.

Lawson, S. J., Selleck, P. W., Galbally, I. E., Keywood, M. D., Harvey, M. J., Lerot, C., Helmig, D., and Ristovski, Z.: Seasonal in situ observations of glyoxal and methylglyoxal over the temperate oceans of the Southern Hemisphere, Atmos. Chem. Phys., 15, 223–240, doi:10.5194/acp-15-223-2015, 2015.

Levy II, H.: Normal atmosphere: large radical and formaldehyde concentrations predicted, Science, 173, 141–143, 1971.

Liang, Q., Jaegle, L., Jaffe, D. A., Weiss, P., Heckman, A., and Snow, J.: Long-range transport to the Northeast Pacific: seasonal variations and transport pathways, J. Geophys. Res., 109, D23S07, doi:10.1029/2003JD004402, 2004.

Mao, J., Jacob, D. J., Evans, M. J., Olson, J. R., Ren, X., Brune, W. H., Clair, J. M. St., Crounse, J. D., Spencer, K. M., Beaver, M. R., Wennberg, P. O., Cubison, M. J., Jimenez, J. L., Fried, A., Weibring, P., Walega, J. G., Hall, S. R., Weinheimer, A. J., Cohen, R. C., Chen, G., Crawford, J. H., McNaughton, C., Clarke, A. D., Jaeglé, L., Fisher, J. A., Yantosca, R. M., Le Sager, P., and Carouge, C.: Chemistry of hydrogen oxide radicals (HO_x) in the Arctic troposphere in spring, Atmos. Chem. Phys., 10, 5823–5838, doi:10.5194/acp-10-5823-2010, 2010.

Mao, J., Paulot, F., Jacob, D. J., Cohen, R. C., Crounse, J. D., Wennberg, P. O., Keller, C. A., Hudman, R. C., Barkley, M. P., and Horowitz, L. W.: Ozone and organic nitrates over the eastern United States: sensitivity to isoprene chemistry, J. Geophys. Res., 118, 11256–11268, doi:10.1002/jgrd.50817, 2013a.

Mao, J., Fan, S., Jacob, D. J., and Travis, K. R.: Radical loss in the atmosphere from Cu-Fe redox coupling in aerosols, Atmos. Chem. Phys., 13, 509–519, doi:10.5194/acp-13-509-2013, 2013b.

McLinden, C. A., Olsen, S. C., Hannegan, B., Wild, O., Prather, M. J., and Sundet, J.: Stratospheric ozone in 3-D models: a simple chemistry and the cross-tropopause flux, J. Geophys. Res., 105, 14653–14665, 2000.

Meinshausen, M., Smith, S. J., Calvin, K., Daniel, J. S., Kainuma, M. L. T., Lamarque, J.-F., Matsumoto, K., Montzka, S. A., Raper, S. C. B., Riahi, K., Thomson, A., Velders, G. J. M., and van Vuuren, D. P. P.: The RCP greenhouse gas concentrations and their extensions from 1765 to 2300, Climatic Change, 109, 213–241, doi:10.1007/s10584-011-0156-z, 2011.

Millet, D. B., Jacob, D. J., Custer, T. G., de Gouw, J. A., Goldstein, A. H., Karl, T., Singh, H. B., Sive, B. C., Talbot, R. W., Warneke, C., and Williams, J.: New constraints on terrestrial and oceanic sources of atmospheric methanol, Atmos. Chem. Phys., 8, 6887–6905, doi:10.5194/acp-8-6887-2008, 2008.

Morgenstern, O., Braesicke, P., O'Connor, F. M., Bushell, A. C., Johnson, C. E., Osprey, S. M., and Pyle, J. A.: Evaluation of the new UKCA climate-composition model – Part 1: The stratosphere, Geosci. Model Dev., 2, 43–57, doi:10.5194/gmd-2-43-2009, 2009.

Morgenstern, O., Zeng, G., Wood, S. W., Robinson, J., Smale, D., Paton-Walsh, C., Jones, N. B., and Griffith, D. W. T.: Long-range correlations in Fourier transform infrared, satellite, and modeled CO in the Southern Hemisphere, J. Geophys. Res., 117, D11301, doi:10.1029/2012JD017639, 2012.

Morgenstern, O., Zeng, G., Abraham, L. N., Telford, P. J., Braesicke, P., Pyle, J. A., Hardiman, S. C., O'Connor, F. M., and Johnson, C. E.: Impacts of climate change, ozone recovery, and increasing methane on surface ozone and the tropospheric oxidizing capacity, J. Geophys. Res., 118, 1028–1041, doi:10.1029/2012JD018382, 2013.

Müller, J.-F. and Stavrakou, T.: Inversion of CO and NO_x emissions using the adjoint of the IMAGES model, Atmos. Chem. Phys., 5, 1157–1186, doi:10.5194/acp-5-1157-2005, 2005.

Müller, J.-F. and Brasseur, G. P.: IMAGES: A three-dimensional chemical transport model of the global troposphere, J. Geophys. Res., 100, 16445–16490, 1995.

Müller, J.-F., Stavrakou, T., Wallens, S., De Smedt, I., Van Roozendael, M., Potosnak, M. J., Rinne, J., Munger, B., Goldstein, A., and Guenther, A. B.: Global isoprene emissions estimated using MEGAN, ECMWF analyses and a detailed canopy environment model, Atmos. Chem. Phys., 8, 1329–1341, doi:10.5194/acp-8-1329-2008, 2008.

Murray, L. T., Jacob, D. J., Logan, J. A., Hudman, R. C., and Koshak, W. J.: Optimized regional and interannual variability of lightning in a global chemical transport model constrained by LIS/OTD satellite data, J. Geophys. Res., 117, D20307, doi:10.1029/2012JD017934, 2012.

Murray, L. T., Logan, J. A., and Jacob, D. J.: Interannual variability in tropical tropospheric ozone and OH: the role of lightning, J. Geophys. Res., 118, 11468–11480, doi:10.1002/jgrd.50857, 2013.

Naik, V., Voulgarakis, A., Fiore, A. M., Horowitz, L. W., Lamarque, J.-F., Lin, M., Prather, M. J., Young, P. J., Bergmann, D., Cameron-Smith, P. J., Cionni, I., Collins, W. J., Dalsøren, S. B., Doherty, R., Eyring, V., Faluvegi, G., Folberth, G. A., Josse, B., Lee, Y. H., MacKenzie, I. A., Nagashima, T., van Noije, T. P. C., Plummer, D. A., Righi, M., Rumbold, S. T., Skeie, R., Shindell, D. T., Stevenson, D. S., Strode, S., Sudo, K., Szopa, S., and Zeng, G.: Preindustrial to present-day changes in tropospheric hydroxyl radical and methane lifetime from the Atmospheric Chemistry and Climate Model Intercomparison Project (ACCMIP), Atmos. Chem. Phys., 13, 5277–5298, doi:10.5194/acp-13-5277-2013, 2013.

Novelli, P. C., Masarie, K. A., and Lang, P. M.: Distributions and recent changes of carbon monoxide in the lower troposphere, J. Geophys. Res., 103, 19015–19034, 1998.

O'Connor, F. M., Johnson, C. E., Morgenstern, O., Abraham, N. L., Braesicke, P., Dalvi, M., Folberth, G. A., Sanderson, M. G., Telford, P. J., Voulgarakis, A., Young, P. J., Zeng, G., Collins, W. J., and Pyle, J. A.: Evaluation of the new UKCA climate-composition model – Part 2: The Troposphere, Geosci. Model Dev., 7, 41–91, doi:10.5194/gmd-7-41-2014, 2014.

Palmer, P. I., Jacob, D. J., Fiore, A. M., Martin, R. V., Chance, K., and Kurosu, T. P.: Mapping isoprene emissions over North America using formaldehyde column observations from space, J. Geophys. Res., 108, 4180, doi:10.1029/2002JD002153, 2003.

Paton-Walsh, C., Deutscher, N. M., Griffith, D. W. T., Forgan, B. W., Wilson, S. R., Jones, N. B., and Edwards, D. P.: Trace gas emissions from savanna fires in northern Australia, J. Geophys. Res., 115, D16314, doi:10.1029/2009JD013309, 2010.

Paulot, F., Crounse, J. D., Kjaergaard, H. G., Kroll, J. H., Seinfeld, J. H., and Wennberg, P. O.: Isoprene photooxidation: new insights into the production of acids and organic nitrates, Atmos. Chem. Phys., 9, 1479–1501, doi:10.5194/acp-9-1479-2009, 2009a.

Paulot, F., Crounse, J. D., Kjaergaard, H. G., Kürten, A., Clair, J. M. S., Seinfeld, J. H., and Wennberg, P. O.: Unexpected epoxide formation in the gas-phase photooxidation of isoprene, Science, 325, 730–733, 2009b.

Pfister, G. G., Emmons, L. K., Hess, P. G., Lamarque, J.-F., Orlando, J. J., Walters, S., Guenther, A., Palmer, P. I., and Lawrence, P. J.: Contribution of isoprene to chemical budgets: a model tracer study with the NCAR CTM MOZART-4, J. Geophys. Res., 113, D05308, doi:10.1029/2007JD008948, 2008.

Pöschl, U., von Kuhlmann, R., Poisson, N., and Crutzen, P.: Development and intercomparison of condensed isoprene oxidation mechanisms for global atmospheric modeling, J. Atmos. Chem., 37, 29–52, doi:10.1023/A:1006391009798, 2000.

Price, C. and Rind, D.: A simple lightning parameterization for calculating global lightning distributions, J. Geophys. Res., 97, 9919–9933, 1992.

Price, C. and Rind, D.: Modeling global lightning distributions in a general-circulation model, Mon. Weather Rev., 122, 1930–1939, 1994.

Price, C., Penner, J., and Prather, M.: NO$_x$ from lightning. 2. Constraints from the global atmospheric electric circuit, J. Geophys. Res., 102, 5943–5951, doi:10.1029/96JD02551, 1997.

Ridley, B., Pickering, K., and Dye, J.: Comments on the parameterization of lightning-produced NO in global chemistry-transport models, Atmos. Environ., 39, 6184–6187, 2005.

Rinsland, C. P., Jones, N. B., Connor, B. J., Logan, J. A., Pougatchev, N. S., Goldman, A., Murcray, F. J., Stephen, M., Pine, A. S., Zander, R., Mahieu, E., and Demoulin, P.: Northern and Southern Hemisphere ground-based infrared spectroscopic measurements of tropospheric carbon monoxide and ethane, J. Geophys. Res., 103, 28197–28217, 1998.

Rinsland, C. P., Jones, N. B., Connor, B. J., Wood, S. W., Goldman, A., Stephen, T. M., Murcray, F. J., Chiou, L. S., Zander, R., and Mahieu, E.: Multiyear infrared solar spectroscopic measurements of HCN, CO, C$_2$H$_6$, and C$_2$H$_2$ tropospheric columns above Lauder, New Zealand (45° S latitude), J. Geophys. Res., 107, ACH 1-1–ACH 1-12, doi:10.1029/2001JD001150, 2002.

Rinsland, C. P., Dufour, G., Boone, C. D., Bernath, P. F., and Chiou, L.: Atmospheric Chemistry Experiment (ACE) measurements of elevated Southern Hemisphere upper tropospheric CO, C$_2$H$_6$, HCN, and C$_2$H$_2$ mixing ratios from biomass burning emissions and long-range transport, Geophys. Res. Lett., 32, L20803, doi:10.1029/2005GL024214, 2005.

Rodgers, C. D. and Connor B. J.: Intercomparison of remote sounding instruments, J. Geophys. Res., 108, 4116, doi:10.1029/2002JD002299, 2003.

Saunders, S. M., Jenkin, M. E., Derwent, R. G., and Pilling, M. J.: Protocol for the development of the Master Chemical Mechanism, MCM v3 (Part A): tropospheric degradation of nonaromatic volatile organic compounds, Atmos. Chem. Phys., 3, 161–180, doi:10.5194/acp-3-161-2003,2003.

Schurgers, G., Arneth, A., Holzinger, R., and Goldstein, A. H.: Process-based modelling of biogenic monoterpene emissions

combining production and release from storage, Atmos. Chem. Phys., 9, 3409–3423, doi:10.5194/acp-9-3409-2009, 2009.

Shim, C., Wang, Y., Choi, Y., Palmer, P. I., Abbot, D. S., and Chance, K.: Constraining global isoprene emissions with Global Ozone Monitoring Experiment (GOME) formaldehyde column measurements, J. Geophys. Res., 110, D24301, doi:10.1029/2004JD005629, 2005.

Shindell, D. T., Faluvegi, G., Stevenson, D. S., Krol, M. C., Emmons, L. K., Lamarque, J.-F., Petron, G., Dentener, F. J., Ellingsen, K., Schultz, M. G., Wild, O., Amann, M., Atherton, C. S., Bergmann, D. J., Bey, I., Butler, T., Cofala, J., Collins, W. J., Derwent, R. G., Doherty, R. M., Drevet, J., Eskes, H. J., Fiore, A. M., Gauss, M., Hauglustaine, D. A., Horowitz, L. W., Isaksen, I. S. A., Lawrence, M. G., Montanaro, V., Müller, J.-F., Pitari, G., Prather, M. J., Pyle, J. A., Rast, S., Rodriguez, J. M., Sanderson, M. G., Savage, N. H., Strahan, S. E., Sudo, K., Szopa, S., Unger, N., van Noije, T. P. C., and Zeng, G.: Multi-model simulations of carbon monoxide: comparison with observations and projected near-future changes, J. Geophys. Res., 111, D19306, doi:10.1029/2006JD007100, 2006.

Staudt, A., Jacob, D., Logan, J., Bachiochi, D., Krishnamurti, T., and Sachse, G.: Continental sources, transoceanic transport, and interhemispheric exchange of carbon monoxide over the Pacific, J. Geophys. Res., 106, 32571–32589, 2001.

Stein, O., Schultz, M. G., Bouarar, I., Clark, H., Huijnen, V., Gaudel, A., George, M., and Clerbaux, C.: On the wintertime low bias of Northern Hemisphere carbon monoxide found in global model simulations, Atmos. Chem. Phys., 14, 9295–9316, doi:10.5194/acp-14-9295-2014, 2014.

Stevenson, D. S., Dentener, F. J., Schultz, M. G., Ellingsen, K., van Noije, T. P. C., Wild, O., Zeng, G., Amann, M., Atherton, C. S., Bell, N., Bergmann, D. J., Bey, I., Butler, T., Cofala, J., Collins, W. J., Derwent, R. G., Doherty, R. M., Drevet, J., Eskes, H. J., Fiore, A. M., Gauss, M., Hauglustaine, D. A., Horowitz, L. W., Isaksen, I. S. A., Krol, M. C., Lamarque, J.-F., Lawrence, M. G., Montanaro, V., Müller, J.-F., Pitari, G., Prather, M. J., Pyle, J. A., Rast, S., Rodriguez, J. M., Sanderson, M. G., Savage, N. H., Shindell, D. T., Strahan, S. E., Sudo, K., and Szopa, S.: Multimodel ensemble simulations of present-day and near-future tropospheric ozone, J. Geophys. Res., 111, D08301, doi:10.1029/2005JD006338, 2006.

Swinnerton, J. W., Linnenbom, V. J., and Lamontagne, R. A.: The ocean: a natural source of carbon monoxide, Science, 167, 984–986, 1970.

Tilmes, S., Lamarque, J.-F., Emmons, L. K., Kinnison, D. E., Ma, P.-L., Liu, X., Ghan, S., Bardeen, C., Arnold, S., Deeter, M., Vitt, F., Ryerson, T., Elkins, J. W., Moore, F., Spackman, J. R., and Val Martin, M.: Description and evaluation of tropospheric chemistry and aerosols in the Community Earth System Model (CESM1.2), Geosci. Model Dev., 8, 1395–1426, doi:10.5194/gmd-8-1395-2015, 2015.

van der Werf, G. R., Randerson, J. T., Giglio, L., Collatz, G. J., Mu, M., Kasibhatla, P. S., Morton, D. C., DeFries, R. S., Jin, Y., and van Leeuwen, T. T.: Global fire emissions and the contribution of deforestation, savanna, forest, agricultural, and peat fires (1997–2009), Atmos. Chem. Phys., 10, 11707–11735, doi:10.5194/acp-10-11707-2010, 2010.

Velazco, V., Wood, S. W., Sinnhuber, M., Kramer, I., Jones, N. B., Kasai, Y., Notholt, J., Warneke, T., Blumenstock, T., Hase, F.,

Murcray, F. J., and Schrems, O.: Annual variation of strato-mesospheric carbon monoxide measured by ground-based Fourier transform infrared spectrometry, Atmos. Chem. Phys., 7, 1305–1312, doi:10.5194/acp-7-1305-2007, 2007.

Vigouroux, C., Hendrick, F., Stavrakou, T., Dils, B., De Smedt, I., Hermans, C., Merlaud, A., Scolas, F., Senten, C., Van-haelewyn, G., Fally, S., Carleer, M., Metzger, J.-M., Müller, J.-F., Van Roozendael, M., and De Mazière, M.: Ground-based FTIR and MAX-DOAS observations of formaldehyde at Réu-nion Island and comparisons with satellite and model data, At-mos. Chem. Phys., 9, 9523–9544, doi:10.5194/acp-9-9523-2009, 2009.

Wai, K. M., Wu, S., Kumar, A., and Liao, H.: Seasonal variability and long-term evolution of tropospheric composition in the trop-ics and Southern Hemisphere, Atmos. Chem. Phys., 14, 4859–4874, doi:10.5194/acp-14-4859-2014, 2014.

Washenfelder, R. A., Toon, G. C., Blavier, J.-F., Yang, Z., Allen, N. T., Wennberg, P. O., Vay, S. A., Matross, D. M., and Daube, B. C.: Carbon dioxide column abundances at the Wisconsin Tall Tower site, J. Geophys. Res., 111, D22305, doi:10.1029/2006JD007154, 2006.

Watson, C. E., Fishman, J., and Reichle Jr., H. G.: The significance of biomass burning as a source of carbon monoxide and ozone in the Southern Hemisphere tropics: a satellite analysis, J. Geophys. Res., 95, 16443–16450, 1990.

Wesely, M. L.: Parameterization of surface resistances to gaseous dry deposition in regional-scale numerical models, Atmos. Envi-ron., 23, 1293–1304, 1989.

Williams, J. E., van Weele, M., van Velthoven, P. F. J., Scheele, M. P., Liousse, C., and van der Werf, G. R.: The impact of uncertainties in african biomass burning emission estimates on modeling global air quality, long range transport and tropo-spheric chemical lifetimes, Atmosphere, 3, 132–163, 2012.

Williams, J. E., van Velthoven, P. F. J., and Brenninkmei-jer, C. A. M.: Quantifying the uncertainty in simulating global tropospheric composition due to the variability in global emis-sion estimates of Biogenic Volatile Organic Compounds, Atmos. Chem. Phys., 13, 2857–2891, doi:10.5194/acp-13-2857-2013, 2013.

Williams, J. E., Le Bras, G., Kukui, A., Ziereis, H., and Bren-ninkmeijer, C. A. M.: The impact of the chemical production of methyl nitrate from the $NO + CH_3O_2$ reaction on the global distributions of alkyl nitrates, nitrogen oxides and tropospheric ozone: a global modelling study, Atmos. Chem. Phys., 14, 2363–2382, doi:10.5194/acp-14-2363-2014, 2014.

Williamson, G. J., Price, O. F., Henderson, S. B., and Bow-man, D. M. J. S.: Satellite-based comparison of fire intensity and smoke plumes from prescribed fires and wildfires in south-eastern Australia, Int. J. Wildland Fire, 22, 121–129, 2013.

Wunch, D., Toon, G. C., Blavier, J.-F. L., Washenfelder, R. A., Notholt, J., Connor, B. J., Griffith, D. W. T., Sherlock, V., and Wennberg, P. O.: The Total Carbon Column Observing Network (TCCON), Phil. Trans. R. Soc. A, 369, 2087–2112, doi:10.1098/rsta.2010.0240, 2011.

Yarwood, G., Rao, S., Yocke, M., and Whitten, G.: Updates to the carbon bond chemical mechanism: CB05, Final report to the US EPA, EPA Report Number: RT-0400675, available at: www.camx.com, 2005.

Zeng, G., Pyle, J. A., and Young, P. J.: Impact of climate change on tropospheric ozone and its global budgets, Atmos. Chem. Phys., 8, 369–387, doi:10.5194/acp-8-369-2008, 2008.

Zeng, G., Wood, S. W., Morgenstern, O., Jones, N. B., Robinson, J., and Smale, D.: Trends and variations in CO, C_2H_6, and HCN in the Southern Hemisphere point to the declining anthropogenic emissions of CO and C_2H_6, Atmos. Chem. Phys., 12, 7543–7555, doi:10.5194/acp-12-7543-2012, 2012.